

To appear in The Astrophysical Journal Supplements

An X-ray Atlas of Groups of Galaxies

John S. Mulchaey

*The Observatories of The Carnegie Institution of Washington, 813 Santa Barbara St., Pasadena,
California 91101*

`mulchaey@ociw.edu`

David S. Davis

*Joint Center for Astrophysics, University of Maryland at Baltimore County and Laboratory for
High Energy Astrophysics/ Goddard Space Flight Center, Code 661.0, Greenbelt, MD 20771*

`ddavis@milkyway.gsfc.nasa.gov`

Richard F. Mushotzky

Laboratory for High Energy Astrophysics, NASA/GSFC, Code 662, Greenbelt, MD 20771

`mushotzky@heavx.dnet.nasa.gov`

and

David Burstein

*Department of Physics and Astronomy, Box 871054, Arizona State University, Tempe, Arizona
85287-1504*

`burstein@samuri.la.asu.edu`

ABSTRACT

A search was conducted for a hot intragroup medium in 109 low-redshift galaxy groups observed with the ROSAT PSPC. Evidence for diffuse, extended X-ray emission is found in at least 61 groups. Approximately one-third of these detections have not been previously reported in the literature. Most of the groups are detected out to less than half of the virial radius with ROSAT. Although some spiral-rich groups do contain an intragroup medium, diffuse emission is restricted to groups that contain at least one early-type galaxy.

Subject headings: galaxies:clusters:general—X-rays: galaxies: clusters

1. Introduction

Most galaxies in the local universe, including our own Milky Way, are members of poor galaxy groups (Geller & Huchra 1983; Tully 1987; Nolthenius & White 1987). The realization that many groups are X-ray sources has led to considerable interest in these systems over the last decade (Mulchaey et al. 1993; Ponman & Bertram 1993; David et al. 1994; Henry et al. 1995; Pildis, Bregman & Evrard 1995; Doe et al. 1995; Saracco & Ciliegi 1995; Mulchaey et al. 1996a; Ponman et al. 1996; Mulchaey & Zabludoff 1998; Helsdon & Ponman 2000a). The X-ray emission in groups is typically extended on scales of hundreds of kiloparsecs. X-ray spectroscopy suggests the emission mechanism is most likely a combination of thermal bremsstrahlung and line emission. This interpretation requires that the entire volume of groups be filled with a hot, low-density gas often referred to as the intragroup medium in analogy to the intracluster medium found in richer systems.

The existence of an intragroup medium is important for many reasons. The presence of a hot gas halo indicates that many groups are likely real, physical systems and not simply chance superpositions or large-scale filaments viewed edge-on. Assuming the intragroup gas is in hydrostatic equilibrium, the total mass of the group can be estimated (Mulchaey et al. 1993; Ponman & Bertram 1993; Pildis, Bregman & Evrard 1995; Mulchaey et al. 1996a). Based on ROSAT data, the typical group mass is approximately one-tenth the mass of a cluster like Virgo. However, because the number density of X-ray detected groups is considerably higher than the number density of clusters like Virgo, the contribution of X-ray detected groups to the total mass density of the universe is comparable to or greater than that of rich clusters. A comparison of the mass in galaxies and intragroup gas to the total group mass indicates that the known baryonic components typically account for only 10–20% of the total mass (Mulchaey et al. 1993; Ponman & Bertram 1993; Henry et al. 1995; Pildis, Bregman & Evrard 1995; Mulchaey et al. 1996a). This implies that groups are dominated by dark matter. Extrapolating the X-ray surface brightness profiles to the virial radius suggests that most of the baryonic mass in groups is in the intragroup medium. In fact, the intragroup medium may be the dominant baryonic component in the local universe (Fukugita, Hogan & Peebles 1998).

The intragroup medium may also hold important clues into the formation and evolution of large-scale structure. Numerical simulations indicate that in the absence of non-gravitational heating, the density profiles of groups and clusters should be nearly identical (Navarro, Frenk & White 1997). In this simple scenario, the relationships between X-ray luminosity (L_X), X-ray temperature (T) and optical velocity dispersion (σ) are expected to be similar for groups and clusters. There is now considerable evidence for departures from such uniformity (Ponman, Cannon & Navarro 1999; Lloyd-Davies, Ponman & Cannon 2000; Mahdavi et al. 2000; Helsdon & Ponman 2000a). The interpretation of these departures is currently a topic of much debate. One possibility is that preheating of the intragroup medium by an early generation of stars can explain the scaling relationships (Cavaliere, Menci & Tozzi 1998; Ponman, Cannon & Navarro 1999; Pierre, Bryan & Gastaud 2000; Finoguenov, David & Ponman 2000; Bialek, Evrard & Mohr 2001; Borgani et al.

2001). Alternative explanations include heating by active galaxies (Valageas & Silk 1999; Fujita & Takahara 2000; Yamada & Fujita 2001), internal heating mechanisms (Loewenstein 2000) and the possibility that galaxy formation is more efficient in groups than in clusters (Bryan 2000).

Most of our current understanding of the intragroup medium is based on observations of groups with ROSAT. The low internal background, large field of view, and good sensitivity to soft X-rays made the ROSAT PSPC detectors ideal instruments for studies of nearby groups. Unfortunately, large systematic surveys of well-selected groups were not performed during the limited lifetime of the PSPC detectors. However, a large number of groups were observed serendipitously. Although ROSAT results have been reported for many of these groups, a significant fraction of the groups in the ROSAT database have not been previously published. Furthermore, the derived X-ray properties of groups are somewhat sensitive to assumptions made during the data reduction and analysis. For this reason, different authors often derive vastly different results from the same ROSAT dataset. Therefore, constructing large samples from the literature can be problematic. In an attempt to produce a more uniform sample, we have reanalyzed the ROSAT PSPC data for all poor groups previously reported in the literature along with a large number of nearby groups that have not previously been published.

We describe the sample selection in §2 and the data reduction in §3. For those groups with detected diffuse emission, we have extracted an X-ray spectrum (§4). Fits to the surface brightness profiles of the groups are described in §5. In §6 we examine the morphological composition of the X-ray detected groups. Finally, a summary is provided in §7.

2. Sample

The ROSAT mission consisted of two main scientific phases, a six-month, all-sky survey with a mean exposure time of approximately 400 seconds and longer pointings of individual targets (the so-called ‘pointed mode’). While the all-sky survey data are deep enough to detect the most X-ray luminous groups (Ebeling, Voges & Böhringer 1994; Henry et al. 1995; Mahdavi et al. 1997, 2000), it is not possible to carry-out detailed spatial and spectral studies with this dataset. As the ‘pointed mode’ observations allow more detailed studies, we restrict our analysis to groups observed during this phase of the ROSAT mission.

We select our groups from a number of different sources. We start by including all groups that were in previous ROSAT ‘pointed-mode’ studies. Many of the groups come from the compact group catalog of Hickson (1982) or from the loose group studies of Mulchaey et al. (1996a), Mulchaey & Zabludoff (1998) and Helsdon & Ponman (2000a). Additional targets were found by cross-correlating the ROSAT observation log with the positions of optically-selected groups in the catalogs of Huchra & Geller (1982), Geller & Huchra (1983), Maia, Da Costa & Latham (1989), Nolthenius (1993) and Garcia (1993). These catalogs also include richer galaxy systems (i.e. clusters). For the purpose of this paper, we only include “groups” with velocity dispersions

less than 600 km/s or an intragroup medium temperature less than 2 keV. A few of the systems we have encountered satisfy one, but not the other criterion. We have opted to include these systems in our sample. In general, we only include groups whose centers fall within 20' of the center of the ROSAT field. The only exceptions are a few Hickson Compact Groups, which were previously included in Ponman et al. (1996) and are included here for comparison. We have not included HCG 73 in our sample, as it is right at the edge of the ROSAT field. We also eliminated any groups that are projected in front of or behind rich clusters.

The final sample of 109 groups is given in Table 1. The name of each group is given in the first column, followed by the Right Ascension and Declination (columns 2 and 3), the number of cataloged galaxies (column 4), redshift (column 5) and velocity dispersion (column 6). For groups with extended X-ray emission, the right ascensions and declinations are generally given for the peak of the X-ray emission, which was determined in each case from the ROSAT image smoothed with a Gaussian profile of width 30". For a few X-ray detected groups, no clear flux peak exists. In these cases, the coordinates refer to the approximate center of the emission morphology. For the non-detected groups, we adopt the coordinates given in the optical group catalogs. Column 7 gives the spiral fraction, defined as the fraction of cataloged members that are late-type galaxies (i.e. spirals and irregulars). We note that the quantities listed in Table 1 have not been calculated to a single minimum absolute magnitude. For most of the groups, the number of members, velocity dispersion and spiral fractions are based on the few brightest ($\sim L_*$) galaxies in the original redshift surveys. However, a few groups have morphologies and membership data down to significantly lower luminosities (Zabludoff & Mulchaey 1998; Mahdavi et al. 1999). Therefore, some caution should be used when comparing the optical properties of individual groups. Column 8 gives the references for the quantities in columns 2-7. The last column gives the cross references for the group in optical group catalogs.

3. Data Reduction and Analysis

To search for a hot intragroup medium, we follow the reduction method outlined in Mulchaey & Zabludoff (1998). First, to remove times of high particle background, we discard any data taken when the master veto rate is greater than 170 counts s^{-1} . For each ROSAT observation, six images are created corresponding to the R2-R7 energy bands given in Snowden et al. (1994). Each of these images is corrected for vignetting using energy-dependent exposure maps. These individual images are combined to produce two final images; one corresponding to the “standard” energy range ~ 0.45 –2.05 keV used in our previous analysis (Mulchaey et al. 1996a; Mulchaey & Zabludoff 1998) and one that includes the “softer” energy bands (~ 0.15 –2.05 keV). We created the softer energy band images with the hope of detecting very cool intragroup gas not visible in the standard images. However, in all cases where emission was found in the softer images, it was also detected in the standard image. Given that the background level is much higher in the softer energy bands, all the analysis presented in this paper is based on the standard images.

Before searching for diffuse intragroup gas, we remove emission associated with point sources. Point sources are identified using the task “DETECT” in the Extended Object and X-ray Background Analysis software (Snowden et al. 1994). We note that in the present context, “point source” refers to a source that appears point-like at the resolution of the ROSAT PSPC (FWHM $\sim 30''$ on-axis and considerably worse off-axis). Emission from point sources is removed by excluding a circular region around each source with a radius 1.5 times the radius that encircles 90% of the source flux. This exclusion radius corresponds to $1.5'$ for sources on-axis (Hassinger et al. 1992). In a few cases, it was necessary to use a slightly larger aperture to remove the flux of more extended sources in the field (such as a very nearby galaxy or a background cluster of galaxies). In most cases where diffuse emission is detected, the emission is centered on a luminous elliptical or S0 galaxy. While the “DETECT” software will usually identify the peak of the extended emission as a “point source” we do not exclude the emission in these cases.

A small fraction of the groups were observed by ROSAT in multiple pointings. In these cases, we reduced the data for each pointing as described above and then combined the images before running the task “DETECT” .

Once the point source emission is removed, the unsmoothed images are examined to determine if a diffuse emission component is present. In addition to a visual inspection, we also create an azimuthally-averaged surface brightness profile for each group to determine if there is excess emission above the background level. Finally, we estimate the excess group counts by adding up the total counts within a radius of $200 h_{100}^{-1}$ kpc of the group center and subtracting the vignetting-corrected background counts estimated from an outer region of the field. In all cases where the visual inspection implied the presence of diffuse emission, both the surface brightness profile and excess count rate are consistent with the existence of intragroup gas. Furthermore, in all cases where the surface brightness profile suggested the presence of diffuse gas, the visual inspection also indicated a diffuse component.

The results of our diffuse emission search and the spectral properties of the diffuse gas are summarized for each group in Table 2. The second column in Table 2 gives the total useful ROSAT exposure time in seconds. The third column indicates whether diffuse emission was detected or not. Groups that clearly show evidence for diffuse emission are labeled “DE” (for diffuse emission), while the non-detected groups are labeled “UL” (for upper limit). A few of the groups that contain a diffuse component also contain a significant contribution from a central AGN. These hybrid objects are labeled “DE/AGN” in Table 2. For a few groups, emission is detected, but the nature of the emission is such that it might not be associated with the group or might not be truly diffuse. These cases are labeled “DE?” in column 3. In HCG 33, a very faint diffuse component is detected, but it is offset from the optical center of the group by nearly $18.5'$ (approximately 400 kpc). Thus, it is unclear whether this emission is associated with the group or a foreground/background object. There are several patches of diffuse emission in the field of HCG 22, but the brightest emission is centered on the background galaxy NGC 1192 and therefore most likely not associated with HCG 22. Several other groups (HCG 15, HCG 35, HCG 48, HCG 57) are clearly detected in the ROSAT

image, but are so far off-axis that it is not possible to cleanly separate an intragroup gas component from emission associated with individual galaxies. Column 4 in Table 2 lists the Galactic neutral column density towards the line of sight as given in Dickey & Lockman (1990), while column 5 gives the maximum radius of X-ray detection determined from examining the surface brightness profile of each group. Columns 6 and 7 give the temperature and metal abundance, respectively, derived from fits to the ROSAT spectra (see §4). The distance to each group (column 8) has been calculated from the recessional velocity with a correction for infall to Virgo and the Great Attractor (Fixsen et al. 1996). Finally, the bolometric luminosity is given in the last column in Table 2.

In Figure 1, we overlay contours of the X-ray emission on the STScI Digitized Sky Survey images for all groups that show evidence for diffuse emission. As has been noted in previous studies (Mulchaey et al. 1996a; Mulchaey & Zabludoff 1998; Helsdon & Ponman 2000a), the diffuse X-ray emission in groups is almost always peaked on an elliptical or S0 galaxy. The emission associated with the central galaxy has been included in Figure 1 except for the cases where an AGN component clearly dominates. All other emission due to point sources in the field has been removed.

Most of the groups in our survey have round, symmetrical morphologies. These morphologies are consistent with the groups being virialized. However, some groups have very irregular, clumpy morphologies that are not centered on any particular galaxy (e.g. HCG 16, HCG 37, SHK 202, NGC 7777). These groups are likely not virialized (Zabludoff & Mulchaey 1998; Dos Santos & Mamon 1999). Five groups have clearly defined bi-modal X-ray distributions (NGC 507, NGC 1407, NGC 3607, NGC 4065 and NGC 7619). In all these cases, the second X-ray peak is also centered on a luminous early-type galaxy. These objects could be groups in the process of merging. Several of the high redshift X-ray groups discovered in the deep Chandra pointing of the Hubble Deep Field North also show evidence for bi-modal X-ray morphologies (Bauer et al. 2002). Although the number of high redshift groups is too small to make any concrete statements, the HDF North data suggests that bi-modal groups may be more common at high redshift (bi-modal groups make up less than 10% of our X-ray detected groups). This idea should be testable in the near future as many more high redshift groups are discovered in deep Chandra and XMM-Newton pointings.

4. Spectral Analysis

For each group with a diffuse emission component, we have attempted to extract a spectrum. The spectra are extracted using a radius that corresponds to the maximum radius of detection determined from examining the surface brightness profile of each group (R_X ; see column 5 in Table 2). Point sources are excluded from the spectrum using the exclusion radii described above (§3). The vignetting-corrected background is estimated in most cases from an annulus with inner radius $36'$ and outer radius $42'$. In a few cases, a different background region is used to avoid the presence of a luminous cluster of galaxies.

To derive the spectral properties of the diffuse gas, we fit the spectra using the software

package XSPEC. For those groups with multiple ROSAT pointings, we fit the individual spectra from each pointing simultaneously. We fit the spectra with an absorbed MEKAL plasma model (Mewe, Gronenschild & van den Oord 1985; Kaastra & Mewe 1993; Liedahl, Osterheld & Goldstein 1995). We fix the absorbing column at the Galactic value given in Dickey & Lockman (1990). For most of the groups, we are unable to constrain the metallicity of the gas with the ROSAT data. In these cases, we fix the gas metallicity to 0.3 solar. For consistency with previous X-ray studies, we adopt the old photospheric value for the solar Fe abundance. To renormalize to the meteoritic value, our metallicity measurements should be increased by a factor of approximately ~ 1.44 . For those groups with sufficient data to fit the metallicity explicitly, we also perform spectral fits with the metallicity fixed at 0.3 solar.

The quoted errors on the temperature and metallicity measurements are at the 90% confidence level. In the UGC 1651 group, the temperature cannot be adequately constrained and no errors are given. The derived temperatures range from ~ 0.3 keV to over 2 keV ($\sim 3.5 \times 10^6$ K - 2.3×10^7 K), with the vast majority of groups centered around 1 keV ($\sim 1.2 \times 10^7$ K; see Figure 2). Groups cooler than ~ 0.3 keV would be difficult to detect with ROSAT because of the high surface brightness of the X-ray background at these soft energies and heavy absorption by Galactic HI (Mulchaey et al. 1996b). Most systems above 2 keV would normally be considered clusters and were thus eliminated from our original sample. To examine how the derived temperatures depend on the assumed metallicity, we compare the derived temperatures for the groups where both a fixed metallicity and variable metallicity model were used (Figure 3). In general, the temperatures are not very sensitive to the assumed metallicity. An exception to this is the NGC 383 group. In this case, fixing the metallicity at a value of 0.3 solar leads to a temperature over twice that found in the variable abundance case.

In general, there is good agreement between the temperatures we derive and previous studies of the same groups with ROSAT. Figure 4 shows a comparison of the temperatures from our survey with the temperatures in Helsdon & Ponman (2000b). The agreement is good despite the fact that different apertures were used for the spectral extractions in many cases. In particular, the Helsdon & Ponman (2000b) temperatures for most of the Hickson Compact Groups were derived using a fixed physical size on the sky, while we use the maximum radius of detection for our extractions.

There is less agreement between our derived temperatures and those measured with the ASCA X-ray telescope. Figure 5 compares the temperatures derived from these two telescopes for all groups in our survey with published ASCA measurements. While the ROSAT and ASCA measurements are similar for cool groups, there are big differences for hotter systems. Above 1 keV, the ASCA temperatures tend to be higher than the ROSAT temperatures by as much as 50%. This trend has been previously noted by Hwang et al. (1999) and Horner (2001). Given the higher energy resolution and bandpass of ASCA, it seems likely the temperatures from this instrument are more reliable. Future observations with Chandra and XMM-Newton should allow more accurate measurements of the X-ray temperatures in hotter groups.

In Figure 6 we compare the metal abundances derived in our ROSAT survey with abundances derived from ASCA observations. While there is considerable scatter in the plot, both the ROSAT and ASCA data are consistent with sub-solar abundances in most cases. However, the reliability of metallicity measurements with these telescopes have been called into question (Bauer & Bregman 1996; Buote 1999, 2000).

The bolometric luminosity of each detected group was estimated from the best-fit MEKAL model assuming the distance to the group given in column 8 of Table 2. To estimate the errors on the luminosities, we varied the temperature and metallicity over their 90% confidence ranges. For those groups without a metallicity measurement, we assume a metallicity range from 0.0 to 1.0 solar. The luminosities are calculated out to the radius used in the spectral extractions. As this radius is usually a fraction of the virial radius of each group, the true bolometric luminosities for these groups could be substantially higher (Helsdon & Ponman 2000a; Mulchaey 2000; Horner 2001). The bolometric luminosities for the X-ray detected groups in our sample span four orders of magnitude (from $\sim 10^{40}$ to $10^{44} \text{ h}_{100}^{-2} \text{ ergs s}^{-1}$; see Figure 7). A comparison of our estimated bolometric luminosities with the common groups in Helsdon & Ponman (2000b) reveals good agreement (see Figure 8). We also compare our bolometric luminosities with luminosities derived from ASCA observations (Figure 9). In general, the ASCA luminosities are somewhat lower than the ROSAT-derived luminosities. This result is not surprising given that the ASCA luminosities are generally derived from smaller apertures.

Figure 10 plots the virial fraction versus the temperature of the system for the X-ray detected groups in our sample (groups with poorly constrained temperatures have been excluded). This plot indicates that the majority of groups are detected to less than half of the virial radius. There is also a trend for the hotter groups to be detected to a larger fraction of the virial radius (Mulchaey 2000). This trend is important because it suggests that a larger fraction of the gas mass, and thus, X-ray luminosity is detected in the hotter systems. This trend continues to rich clusters of galaxies which are in general detected out to approximately the virial radius (Mulchaey 2000).

For the groups that were not detected, we estimate upper limits on the X-ray luminosities using a method similar to that described in Mulchaey et al. (1996a). First, we measure the net counts (N) and rms error (σ) in a region $200 \text{ h}^{-1} \text{ kpc}$ in radius centered on each group (for a few nearby groups it was necessary to adopt a radius smaller than $200 \text{ h}^{-1} \text{ kpc}$; see Table 2). We then calculate the flux a MEKAL plasma of temperature 1 keV and abundance 0.3 solar would need to produce $N+3\sigma$ (if $N>0$) or 3σ (if $N<0$) counts.

5. Spatial Analysis

For each group with a detected diffuse component we have fit the two-dimensional surface brightness profile using a modified King function (the so-called ‘ β -model’):

$$S(R)=S_o (1.0 + (R/R_{\text{core}})^2)^{-3\beta+0.5}.$$

The model is first convolved with the 1 keV ROSAT PSPC point spread function, and then fit to the data with S_o , R_{core} , β and the position of the center of the emission as free parameters. Following Helsdon & Ponman (2000a), we also fit both circular and elliptical fits. In the latter fits, the ellipticity and position angle are additional free parameters. The results of the elliptical fits are given in Table 3. During the fits, each free parameter was allowed to vary between a reasonable lower and upper bound. For a large number of groups, the best-fit core radius was at the lower bound value ($0.1'$). This value is smaller than the resolution of the ROSAT PSPC. In these cases, the core radius is listed as ' $<0.1'$ ' in Table 3. To determine what effect this lower bound might have on the other derived parameters, we fit a number of groups again without the lower bound. These fits suggest that removing the lower bound on R_{core} has a minimal impact on the derived values of β and ellipticity (see also the similar finding of Helsdon & Ponman (2000a)).

The goodness of each fit was estimated using χ -squared statistics. Because the number of counts in each bin is small, we use the prescription of Gehrels (1986) to calculate the standard deviation. While the single- β models fits provide an adequate description of the images in some cases, in general the fits are poor. Previous studies of X-ray luminous groups indicate that the surface brightness profiles of groups are complicated, often requiring multiple components to adequately describe the data (Mulchaey & Zabludoff 1998; Helsdon & Ponman 2000a). In particular, single King models tend to underestimate the flux at the very centers of luminous groups. Mulchaey & Zabludoff (1998) suggested that groups contain two components, one associated with the central galaxy (the 'central' component) and a second component associated with the group as a whole (the 'extended' component). For those groups in our sample with a sufficient number of counts (~ 1000), we fit the two-dimensional surface brightness profiles with a two-component β model. Initially, we experimented with allowing both components to be elliptical in shape (i.e. let the ellipticity and position angle be free parameters). We found, however, that it was not possible to constrain these fits in most cases. Next, we adapted the procedure used by Helsdon & Ponman (2000a) and allowed one of the components to be elliptical and required the other to be circular. While these models provided adequate fits to some groups, it was often necessary to restrict the number of free parameters even further in some cases. In particular, the β values for the circular models often reached unphysically high values. When this occurred, we fit the surface brightness profiles again with the β value of the core component fixed at a value of 1.0 (Helsdon & Ponman (2000a) encountered a similar problem in their fits; Stephen Helsdon, private communication). In those cases where a double β -model fit was performed, the results are given in Table 3. Note that for the double β -model fits, the elliptical component is always listed first (i.e. the elliptical component is identified as the 'extended component'). In a few cases, this results in the core radius of the 'extended component' being smaller than the core radius of the 'central component'.

Figure 11 shows the distribution of extended component β values for our group sample (we adopt the two component fits where available). The mean value of β for the sample is 0.47 ± 0.16 . This value is in excellent agreement with the weighted mean that Helsdon & Ponman (2000a) find for their sample (0.46 ± 0.06) and is somewhat lower than the typical value found for rich clusters

(Arnaud & Evrard 1999; Mohr, Mathiesen & Evrard 1999).

6. Detection Statistics

The existence of a hot intragroup medium in poor groups of galaxies has been firmly established over the past decade. However, the frequency of diffuse X-ray emission in groups is still rather uncertain. Most previous studies using ROSAT ‘pointed mode’ data have been restricted to rather small samples selected in a potentially biased way. For example, many of the targets in these surveys were a priori known to be bright X-ray sources based on previous detection (i.e. in the ROSAT All-Sky Survey). Furthermore, a significant fraction of the groups studied to date come from the Hickson Compact Group catalog, which may not be representative of groups in general (see, however Helsdon & Ponman (2000b)). Mahdavi et al. (2000) attempted to overcome these problems by looking for X-ray emission in the ROSAT All-Sky Survey data for a large sample of groups selected from the CfA redshift survey. Correcting for selection effects, Mahdavi et al. (2000) estimate that approximately 40% of groups are extended X-ray sources.

Our present survey represents the largest sample of groups studied to date with ROSAT PSPC ‘pointed mode’ data. Diffuse emission is detected in at least 61 of the 109 groups (56%) in our sample (not counting the 6 questionable detections) down to the detection limits of our survey. Unfortunately, our sample is plagued by the same biasing issues that effect the earlier pointed mode studies. A deep X-ray survey of a large, optically-selected group sample should be a priority for the current generation of X-ray telescopes.

Early studies of groups with ROSAT suggested that X-ray emission is largely restricted to systems with low spiral fractions (Ebeling, Voges & Böhringer 1994; Pildis, Bregman & Evrard 1995; Mulchaey et al. 1996a). However, Ponman et al. (1996) found that some spiral-rich groups do indeed contain X-ray emission. Figure 12 shows the distribution of spiral-fractions for our entire sample and for the X-ray detected groups. This figure is consistent with Ponman et al. (1996)’s suggestion that some spiral-rich groups are X-ray detected. Interestingly, however, all of the groups with a detectable intragroup medium contain at least one early-type galaxy. Therefore, the ROSAT data are consistent with no spiral-only groups containing a detectable hot intragroup medium.

Several explanations for the failure to detect spiral groups in X-rays have been proposed. One possibility is that spiral-only groups are not real, physical systems, but rather chance superpositions of galaxies along the sight. However, our own Local Group would be defined as “spiral-only” if it was placed at the distance typical of the groups in our survey (Zabludoff & Mulchaey 1998). Therefore, this possibility seems unlikely. Another possibility is that the gas density is significantly lower in spiral-only groups. Lower gas density in spiral groups may in fact be consistent with expectations from recent preheating models (Ponman, Cannon & Navarro 1999). The temperature of the gas in spiral-only groups may also be too cool to produce detectable X-ray emission (Mulchaey et al. 1996b). Based on their velocity dispersions, the virial temperatures of spiral-only groups do

tend to be lower than those of their early-type dominated counterparts. A “warm” intragroup medium might produce detectable features in the far-ultraviolet or X-ray spectra of background quasars (Mulchaey et al. 1996b; Perna & Loeb 1998; Hellsten, Gnedin & Miralda-Escude 1998). High-ionization absorption line features consistent with cooler groups have recently been reported. For example, Fang et al. (2002) have reported the detection of an O VIII Ly α absorption line associated with a spiral group along the sightline towards PKS 2155-304. Similarly, some of the O VI systems found with HST and FUSE may be consistent with an origin in small galaxy groups (Savage et al. 2002). Further absorption studies should provide insight into the presence of warm intragroup gas in spiral-only groups.

7. Summary

We have searched for diffuse X-ray emission in 109 nearby galaxy groups using data taken with the ROSAT PSPC during its ‘pointed mode’ phase. We find evidence for a hot intragroup medium in approximately half of the groups in our sample. Although we detect many spiral-rich groups, none of the spiral-only groups in our survey show clear evidence for the presence of diffuse X-ray emission. Spiral-only groups may contain intragroup gas, but the temperature or gas density may be too low to produce appreciable X-ray emission.

In general, nearby groups are detected to only a fraction of the virial radius with the ROSAT PSPC. Therefore, a significant amount of the gas mass likely occurs beyond the current X-ray detection radius. Future observations with Chandra and XMM-Newton should provide further insight into the distribution of hot gas in these cosmologically-important systems.

The authors acknowledge useful conversations with Alex Athey, Steven Helsdon, Donald Horner, Trevor Ponman, Ann Zabludoff and Marc Zimer. We also acknowledge Mark Donikian for help with the figures. This project made extensive use of NASA’s HEASARC, NED and Skyview databases. Partial support for this project was provided by NASA grant NAG 5-3529.

REFERENCES

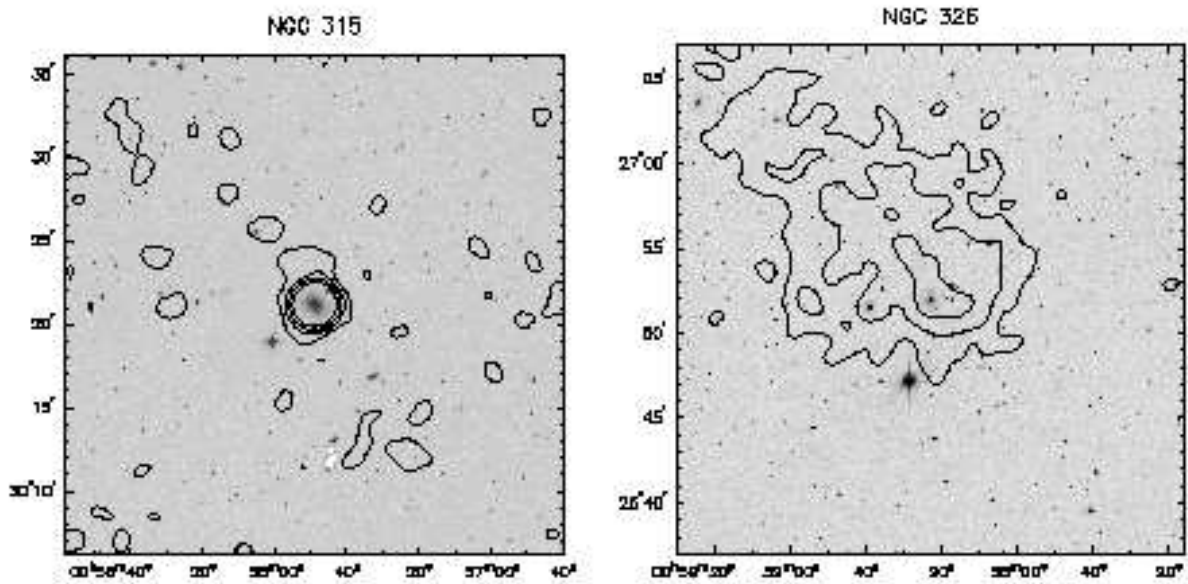
- Arnaud, M., and Evrard, A. E. 1999, MNRAS, 305, 631
- Bauer, F., and Bregman, J. N. 1996, ApJ, 457, 382
- Bauer, F. E., et al. 2002, ApJ, in press
- Bialek, J. J., Evrard, A. E., and Mohr, J. J. 2001, ApJ, 555, 597
- Buote, D. A. 1999, MNRAS, 309, 685

- Buote, D. A. 2000, MNRAS, 311, 176
- Borgani, S. et al. 2001, ApJ, 559, 71
- Bryan, G. L. 2000, ApJ, 544, L1
- Cavaliere, A., Menci, N., and Tozzi, P. 1998, ApJ, 501, 493
- Cowie, L. L., Henriksen, M., and Mushotzky, R. F. 1987, ApJ, 317, 593
- David, L. P., Jones, C., Forman, W., and Daines, S. 1994, ApJ, 428, 544
- Davis, D. S., Mushotzky, R. F., Mulchaey, J. S., Worrall, D. M., Birkinshaw, M., and Burstein, D. 1995, ApJ, 444, 582
- Dickey, J. M., and Lockman, F. J. 1990, ARA&A, 28, 215
- Doe, S. M., Ledlow, M. J., Burns, J. O., and White, R. A. 1995, AJ, 110, 46
- Dos Santos, S., and Mamon, G. A. 1999, A&A, 352, 1
- Ebeling, H., Voges, W., Böhringer, H. 1994, ApJ, 436, 44
- Evrard, A. E., Metzler, C. A., Navarro, J. F. 1996, ApJ, 469, 494
- Fabricant, D., and Gorenstein, P. 1983, ApJ, 267, 535
- Fabricant, D., Lecar, M., and Gorenstein, P. 1980, ApJ, 241, 552
- Fabricant, D., Rybicki, G., and Gorenstein, P. 1984, ApJ, 286, 186
- Fang, T., Marshall, H. L., Lee, J. C., Davis, D. S., and Canizares, C. R. 2002, ApJ, in press
- Finoguenov, A., David, L. P., Ponman, T. J. 2000, ApJ, 544, 188
- Fixsen, D. J., Cheng, E. S., Gales, J. M., Mather, J. C., Shafer, R. A., Wright, E. L. 1996, ApJ, 473, 576
- Fujita, Y., and Takahara, F. 2000, ApJ, 536, 523
- Fukugita, M., Hogan, C. J., and Peebles, P. J. E. 1998, ApJ, 503, 518
- Garcia, A. M. 1993, A&AS, 100, 47
- Gehrels, N. 1986, ApJ, 303, 336
- Geller, M. J., and Huchra, J. P. 1983, ApJS, 52, 61
- Hasinger, G., Turner, T. J., George, I. M., and Boese, G. 1992, NASA/GSFC Office of Guest Investigator Programs, Calibration Memo CAL/ROS92-001

- Hellsten, U., Gnedin, N.Y., and Miralda-Escude, J. 1998, *ApJ*, 509, 56
- Helsdon, S. F., and Ponman, T. J. 2000a, *MNRAS*, 315, 356
- Helsdon, S. F., and Ponman, T. J. 2000b, *MNRAS*, 319, 933
- Henry, J. P., Gioia, I. M., Huchra, J. P., Burg, R., McLean, B., et al. 1995, *ApJ*, 449, 422
- Hickson, P. 1982, *ApJ*, 255, 382
- Hickson, P., Huchra, J., and Kindl, E. 1989, *ApJS*, 70, 687
- Hickson, P., Mendes de Oliveira, C., Huchra, J. P., and Palumbo, G. G. 1992, *ApJ*, 399, 353
- Horner, D. J. 2001, Ph D thesis, U. of Maryland
- Huchra, J. P., and Geller, M. J. 1982, *ApJ*, 257, 423
- Hwang, U., Mushotzky, R. F., Burns, J. O., Fukazawa, Y, White, R. A. 1999, *ApJ*, 516, 604
- Kaastra, J. S., and Mewe, R. 1993, *A&AS*, 97, 443
- Liedahl, D. A., Osterheld, A. L., and Goldstein, W. H. 1995, *ApJ*, 438, L 115
- Lloyd-Davies, E. J., Ponman, T. J., and Cannon, D. B. 2000, *MNRAS*, 315, 689
- Loewenstein, M. 2000, *ApJ*, 532, 17
- Maia, M. A. G., da Costa, L. M., Latham, D. W. 1989, *ApJS*, 69, 809
- Mahdavi, A., Böhringer, H., Geller, M. J., and Ramella, M. 1997, *ApJ*, 483, 68
- Mahdavi, A., Geller, M. J., Böhringer, H., Kurtz, M. J., and Ramella, M. 1999, *ApJ*, 518, 69
- Mahdavi, A., Böhringer, H., Geller, M. J., and Ramella, M. 2000, *ApJ*, 534, 114
- Mewe, R., Gronenschild, E. H. B. M., and van den Oord, G. H. J. 1985, *A&AS*, 35, 503
- Mohr, J. J., Mathiesen, B., and Evrard, A. E. 1999, *ApJ*, 517, 627
- Mulchaey, J. S. 2000, *ARA&A*, 38, 289
- Mulchaey, J. S., Davis, D. S., Mushotzky, R. F., and Burstein, D. 1993, *ApJ*, 404, L9
- Mulchaey, J. S., Davis, D. S., Mushotzky, R. F., and Burstein, D. 1996a, *ApJ*, 456, 80
- Mulchaey, J. S., Mushotzky, R. F., Burstein, D., and Davis, D. S. 1996b, *ApJ*, 456, L5
- Mulchaey, J. S., and Zabludoff, A. I. 1998, *ApJ*, 496, 73
- Navarro, J. F., Frenk, C. S., and White, S. D. M. 1997, *ApJ*, 490, 493

- Nolthenius, R. 1993, *ApJS*, 85, 1
- Nolthenius, R., and White, S. D. M. 1987, *MNRAS*, 225, 505
- Perna, R., and Loeb, A. 1998, *ApJ*, 503, L135
- Pierre, M., Bryan, G., and Gastaud, R. 2000, *A&A*, 356, 403
- Pildis, R. A., Bregman, J. N., and Evrard, A. E. 1995, *ApJ*, 443, 514
- Ponman, T. J., and Bertram 1993, *Nature*, 363, 51
- Ponman, T. J., Bourner, P. D. J., Ebeling, H., Böhringer, H. 1996, *MNRAS*, 283, 690
- Ponman, T. J., Cannon, D. B., and Navarro, J. F. 1999, *Nature*, 397, 135
- Ribeiro, A. L., de Carvalho, R. R., Capelato, H. V., and Zepf, S. E. 1998, *ApJ*, 497, 72
- Saracco, P., and Ciliegi, P. 1995, *A&A*, 301, 348
- Savage, B. D., Sembach, K. R., Tripp, T. M., and Richter, P. 2002, *ApJ*, 564, 631
- Snowden, S. L., McCammon, D., Burrows, D. N., and Mendehall, J. A. 1994, *ApJ*, 424, 714
- Tully, R. B. 1987, *ApJ*, 321, 280
- Valageas, P., and Silk, J. 1999, *A&A*, 350, 725
- Werner, P. N., Worrall, D. M., and Birkinshaw, M. 1999, *MNRAS*, 307, 722
- Willmer, C. N. A., Focardi, P., Chan, R., Pellegrini, P. S., da Costa, N. L. 1991, *AJ*, 101, 57
- Willmer, C. N. A., Maia, M. A. G., Mendes, S. O., Alonso, M. V., Rios, L. A., Chaves, O. L., and de Mello, D. F. 1999, *AJ*, 118, 1131
- Yamada, M., and Fujita, Y. 2001, *ApJ*, 553, L145
- Zabludoff, A. I., and Mulchaey, J. S. 1998, *ApJ*, 496, 39
- Zabludoff, A. I., and Mulchaey, J. S. 2000, *ApJ*, 539, 136
- Zimer, M., Zabludoff, A. I., and Mulchaey, J. S. 2002, in preparation

Fig. 1.— Contour maps of diffuse X-ray emission overlaid on the STScI digitized sky survey for each group detected in our survey. The coordinates are in epoch J2000. Emission from point sources in the field has been removed except for emission associated with the central galaxy. The contours correspond to 3σ , 5σ , 10σ , 20σ and 40σ above the background. The data have been smoothed with a Gaussian of width $30''$. The complete Figure 1 is available at: <http://www.ociw.edu/~mulchaey/Atlas/atlas.html>



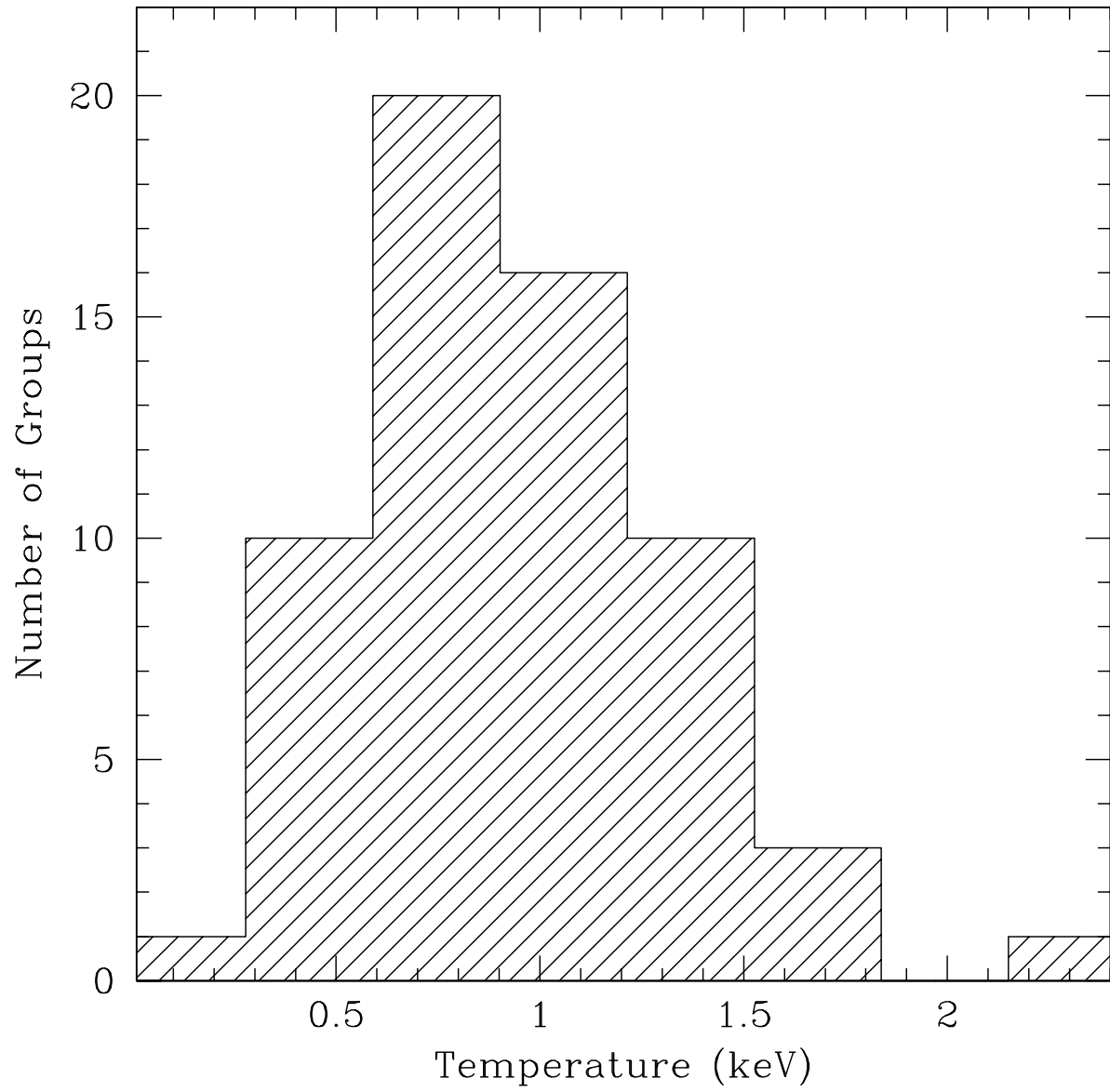


Fig. 2.— Distribution of derived gas temperatures for the group sample.

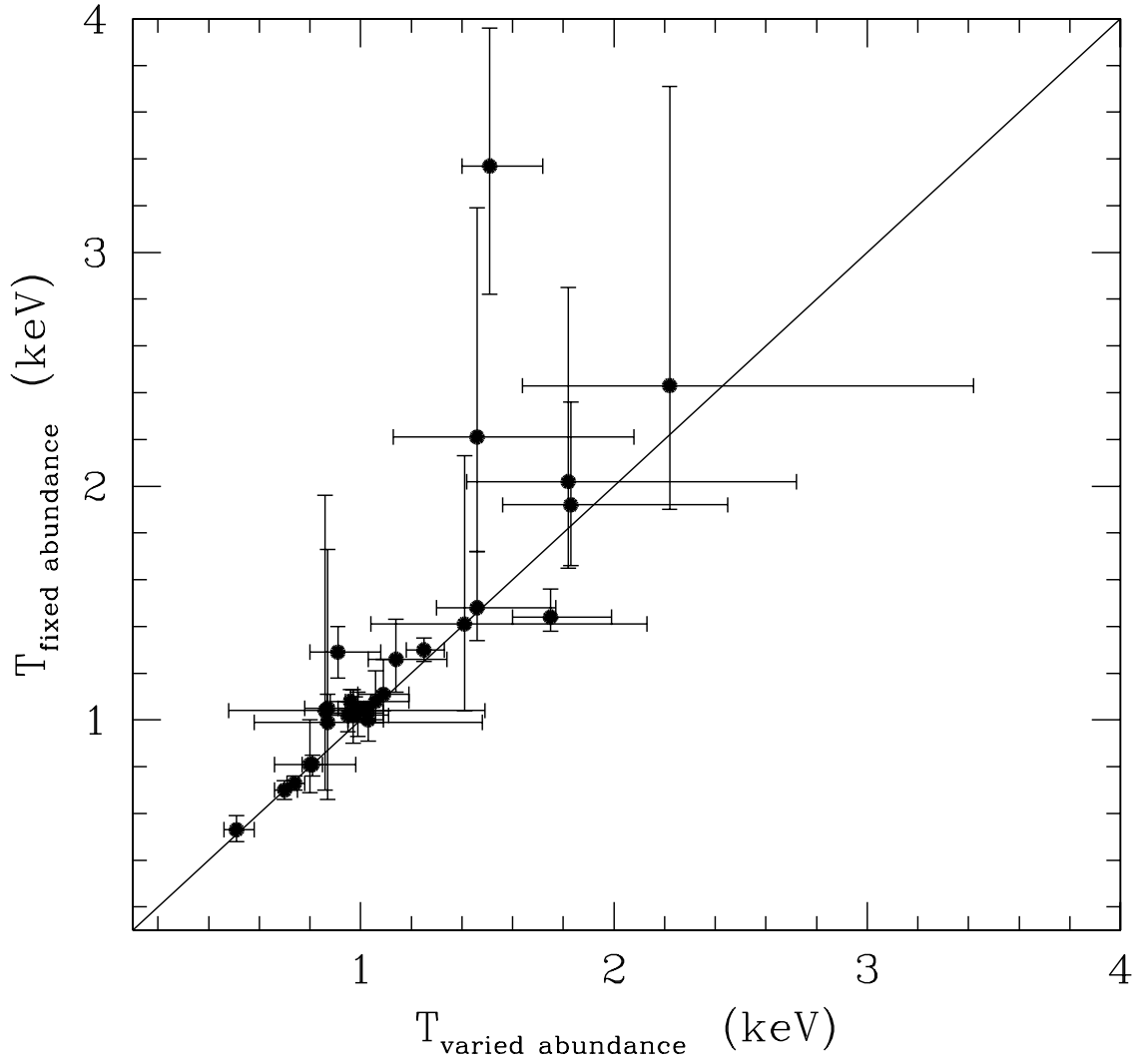


Fig. 3.— A comparison of the ROSAT derived temperatures for a MekaL model with the metallicity allowed to vary versus a MekaL model with the metallicity fixed to 0.3 solar.

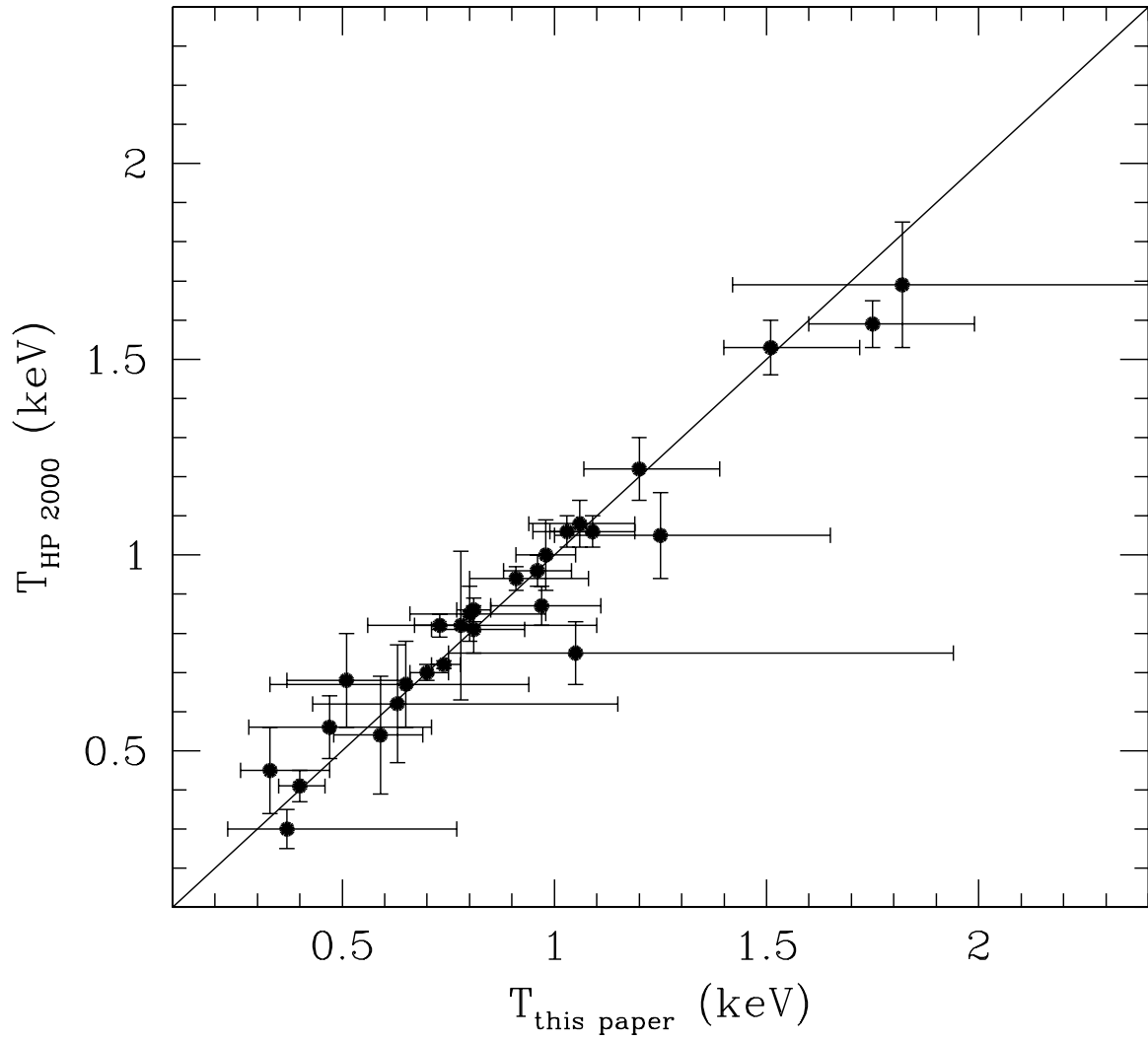


Fig. 4.— A comparison of derived gas temperatures from the present survey with those in Helsdon & Ponman (2000b). Overall, the agreement is very good.

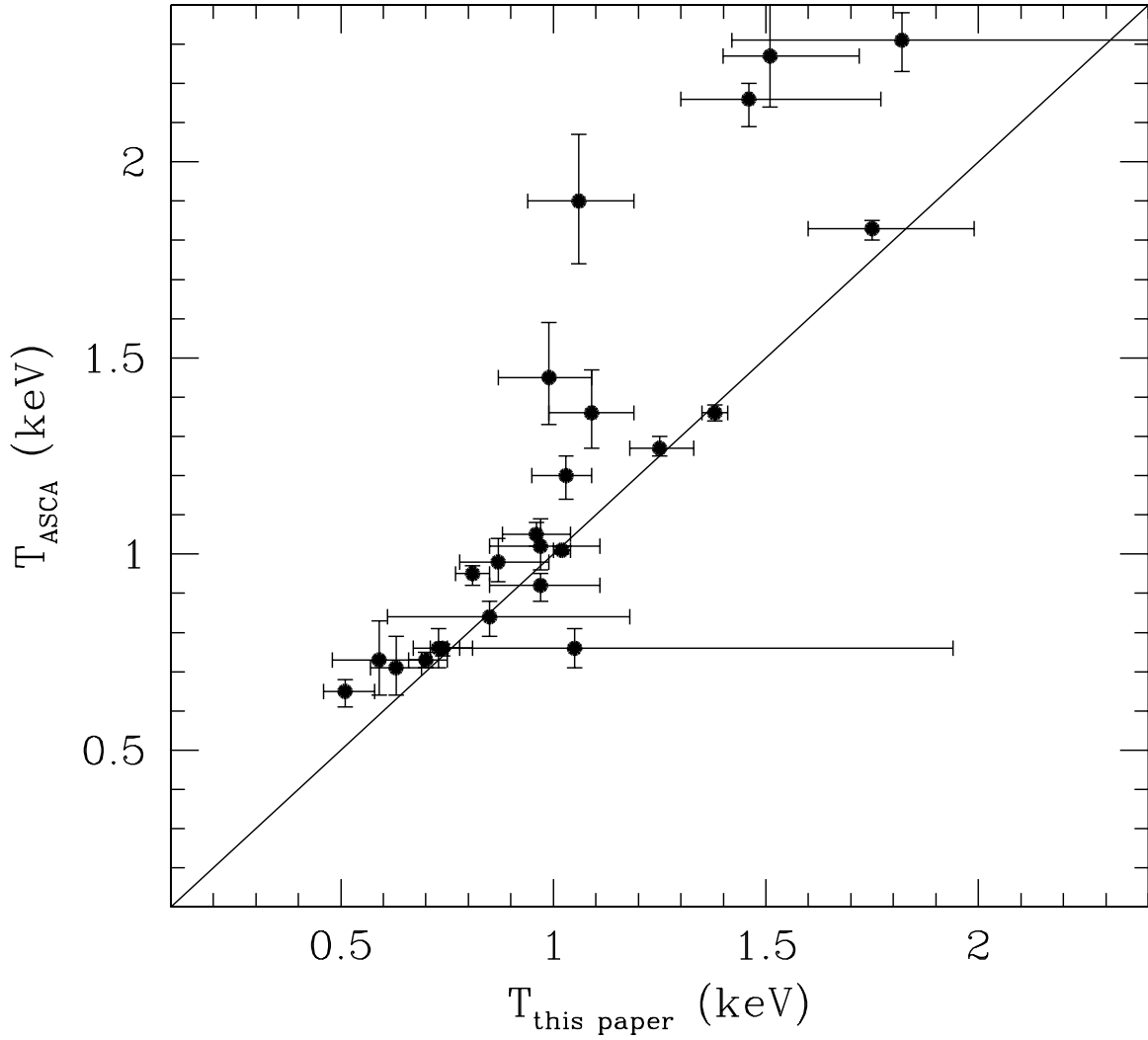


Fig. 5.— A comparison of the best-fit ROSAT derived temperatures with temperature measurements made with the ASCA X-ray telescope. The ASCA measurements are taken from the literature and assume an isothermal MekaL model. There is a trend for the ROSAT data to underestimate the gas temperature especially for temperatures greater than 1 keV.

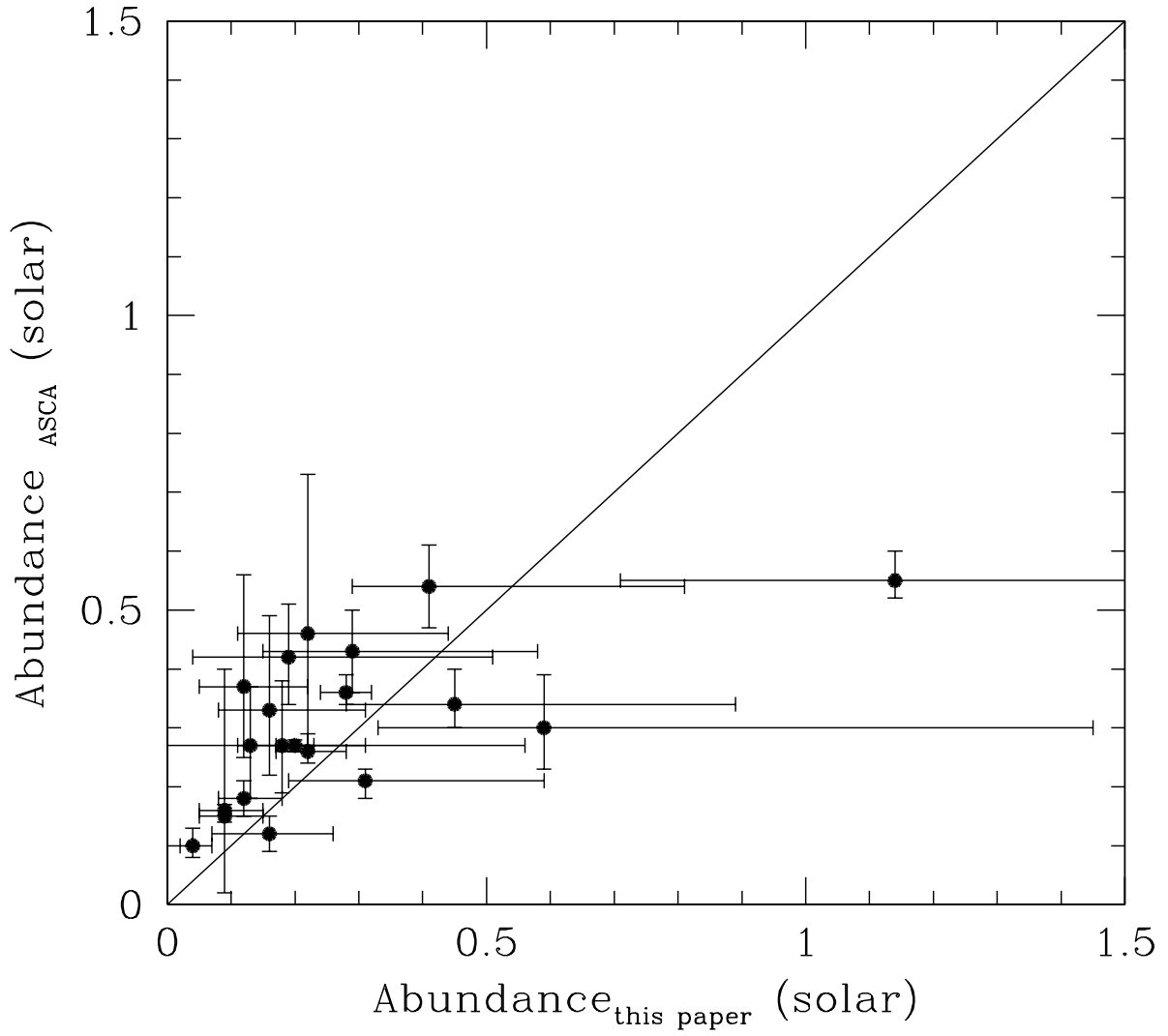


Fig. 6.— A comparison of the best-fit ROSAT derived abundances with abundance measurements made with the ASCA X-ray telescope. The ASCA measurements are taken from the literature and assume an isothermal MekaL model.

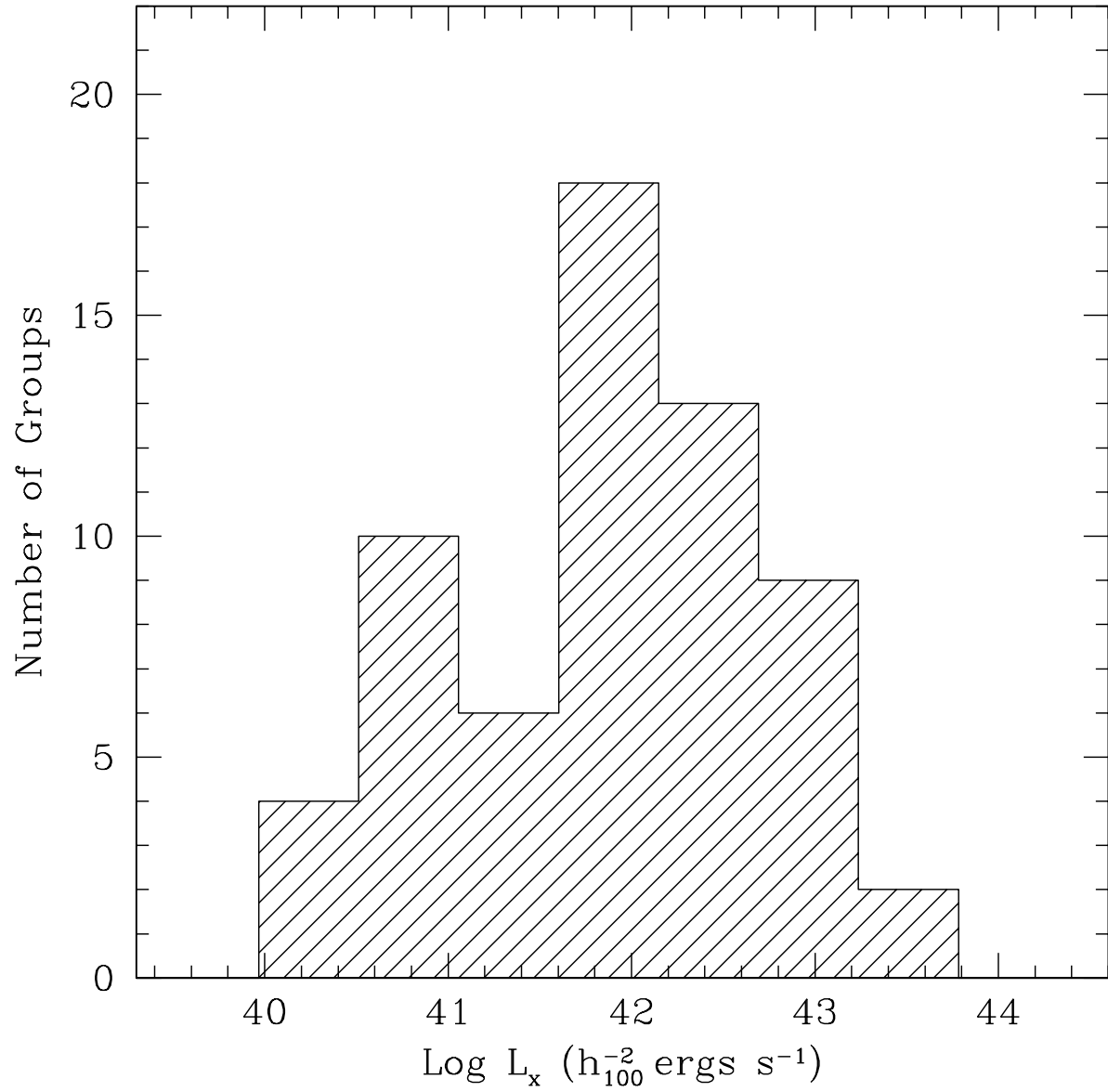


Fig. 7.— Distribution of bolometric luminosities for the groups in the sample with detected extended X-ray emission.

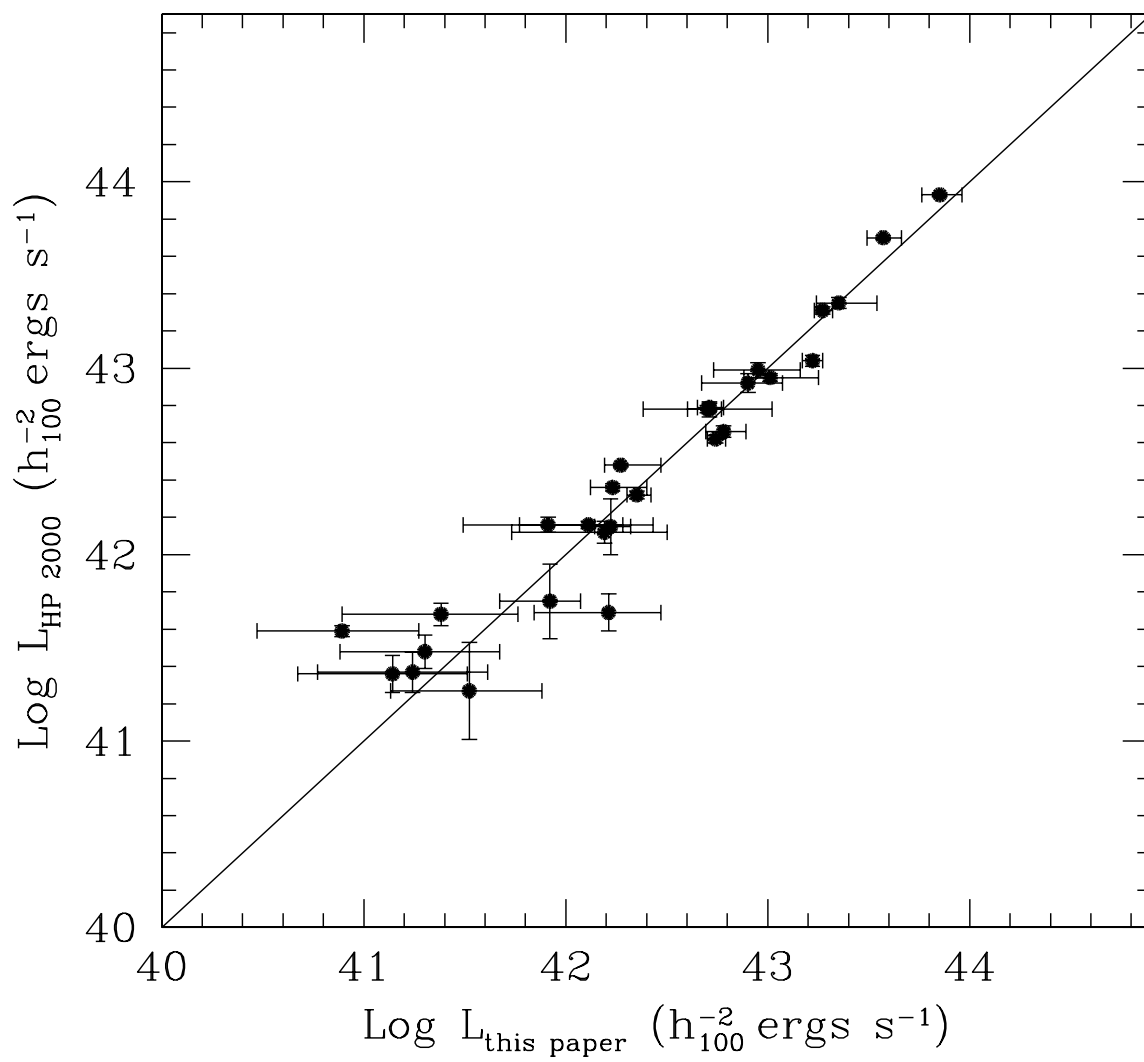


Fig. 8.— A comparison of bolometric luminosities from the present survey with those in Helsdon & Ponman (2000b). Overall, the agreement is very good.

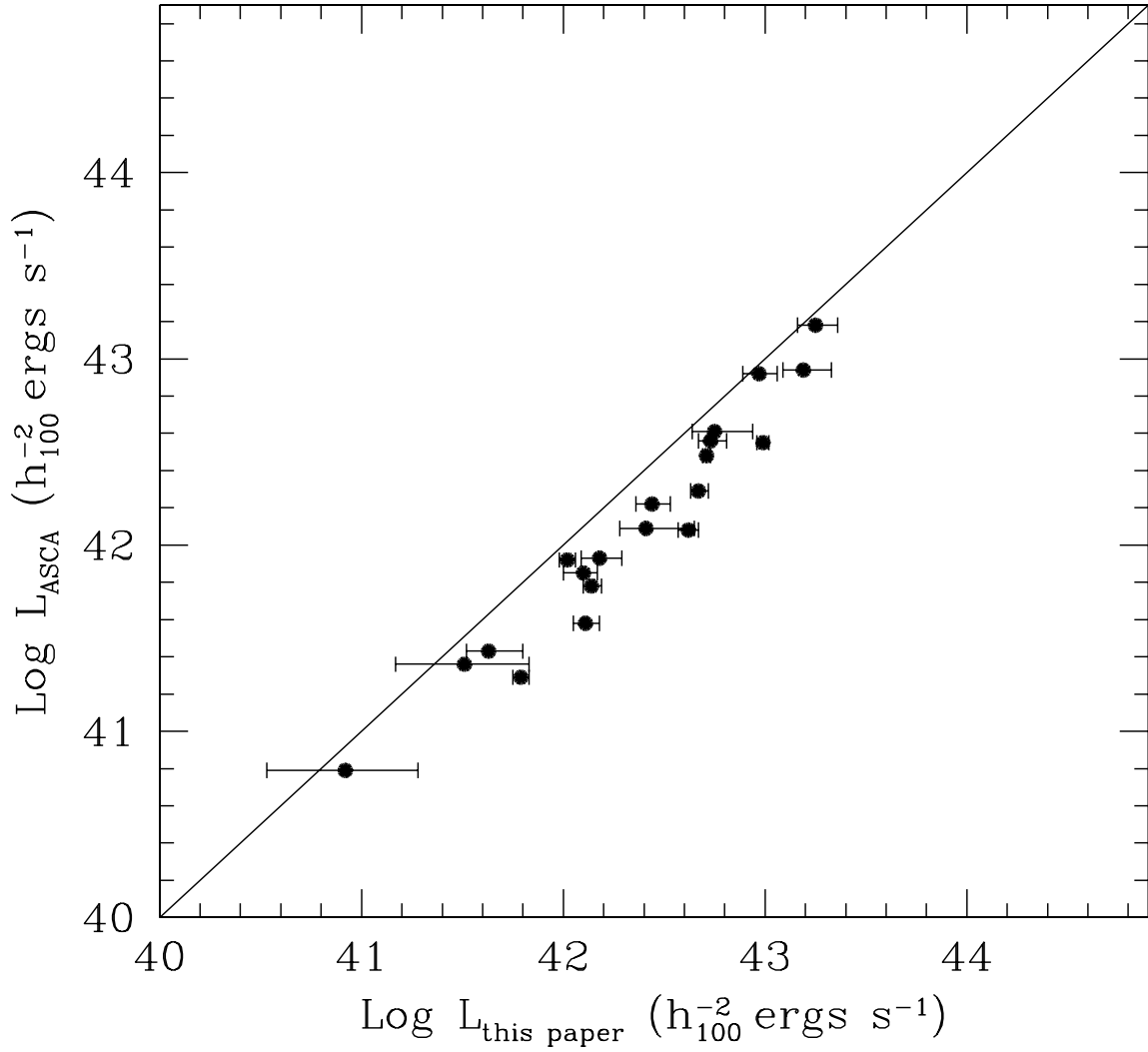


Fig. 9.— A comparison of bolometric luminosities derived from the present survey with bolometric luminosities derived from ASCA observations. The ASCA luminosities tend to be smaller than those derived from the ROSAT data. This is most likely because smaller extraction radii were used in the ASCA analysis.

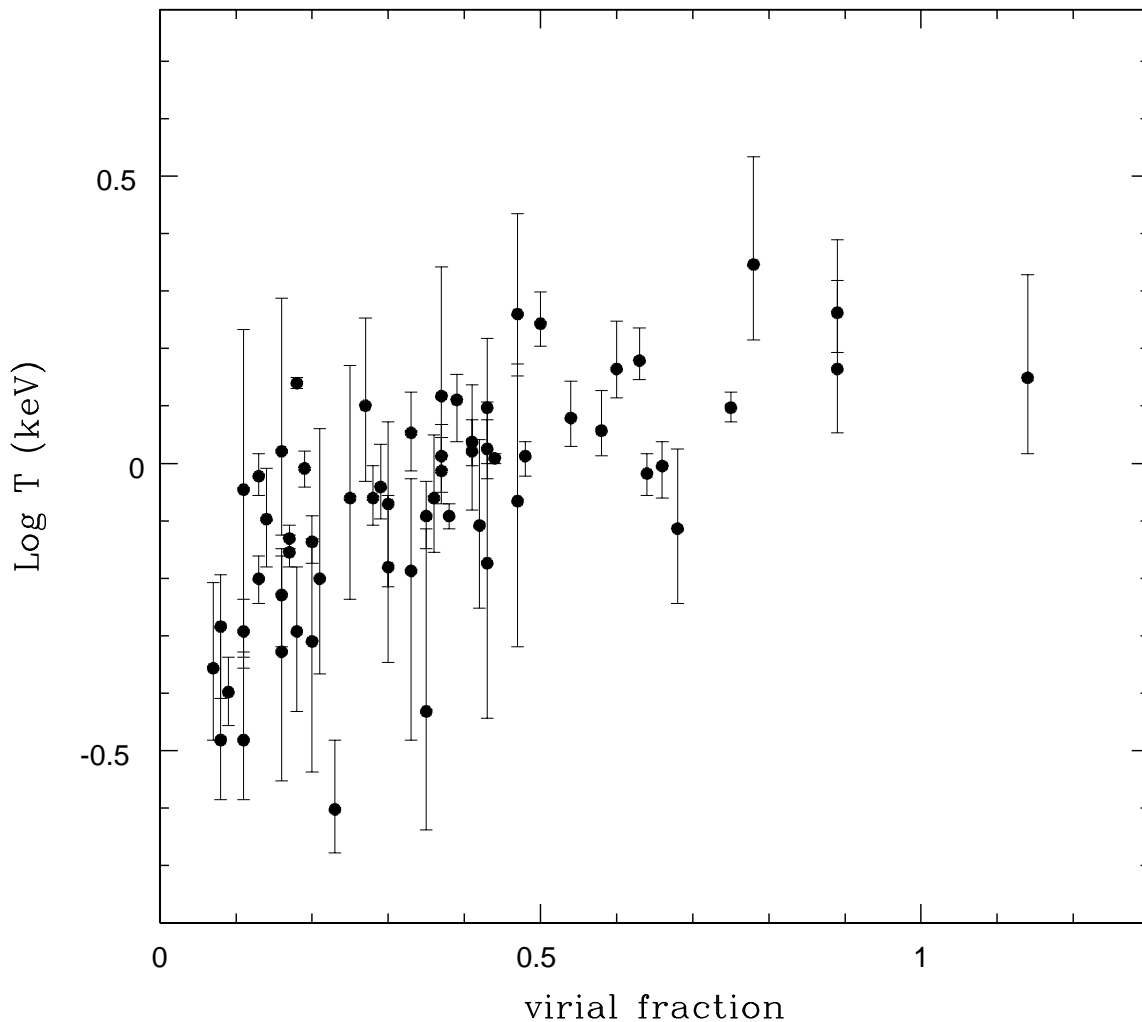


Fig. 10.— Total radius of X-ray extent plotted as a fraction of the virial radius of each system versus the logarithm of the temperature for the group sample. The virial radius for each system was calculated assuming $r_{\text{virial}}(T) = 1.85 (T/10\text{keV})^{0.5} (1+z)^{-1.5} h_{100}^{-1} \text{ Mpc}$ (Evrard et al 1996).

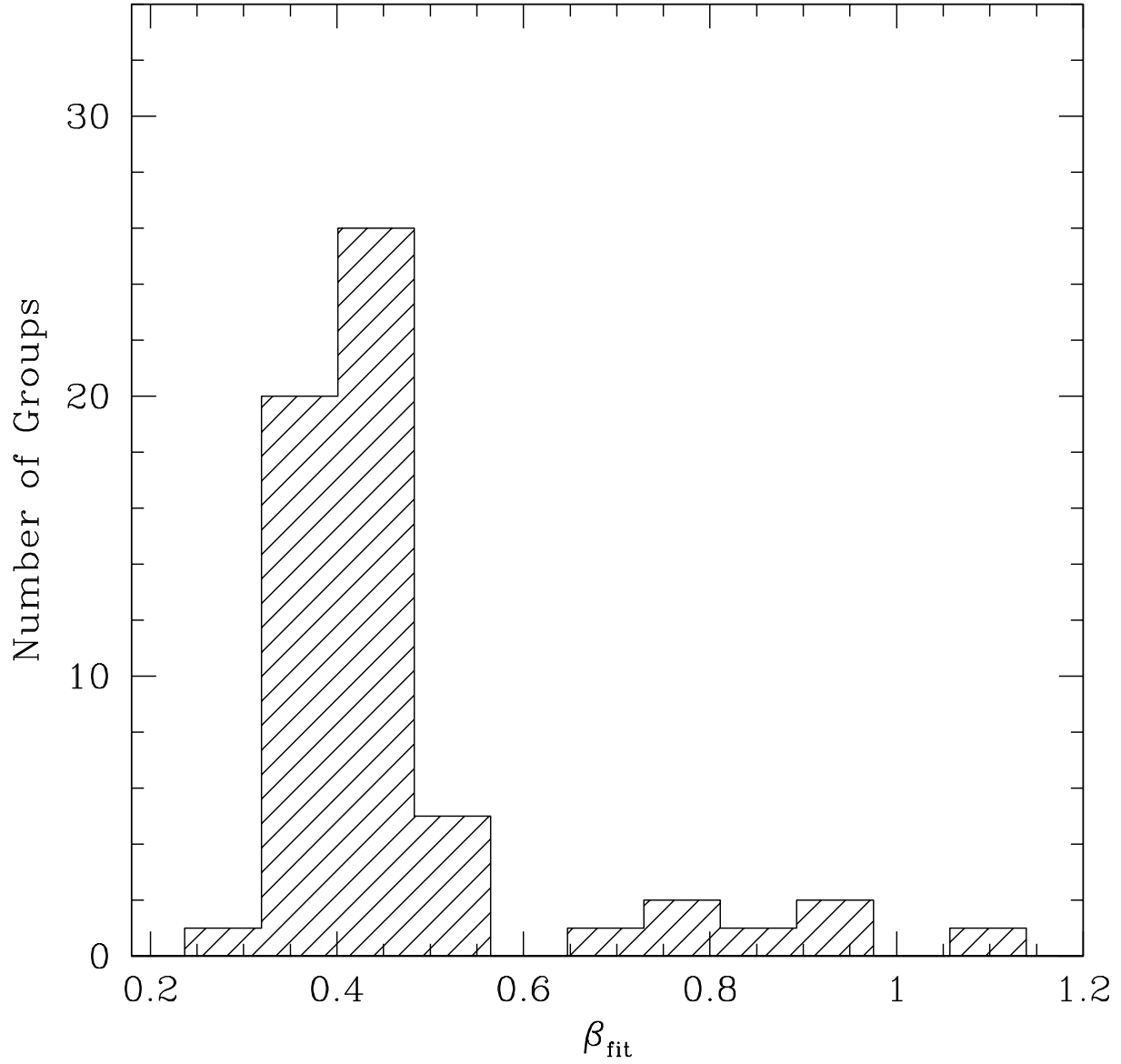


Fig. 11.— Distribution of β values for the extended component derived from β -model fits. The β values are taken from the two component fits where available, otherwise the single component value is used.

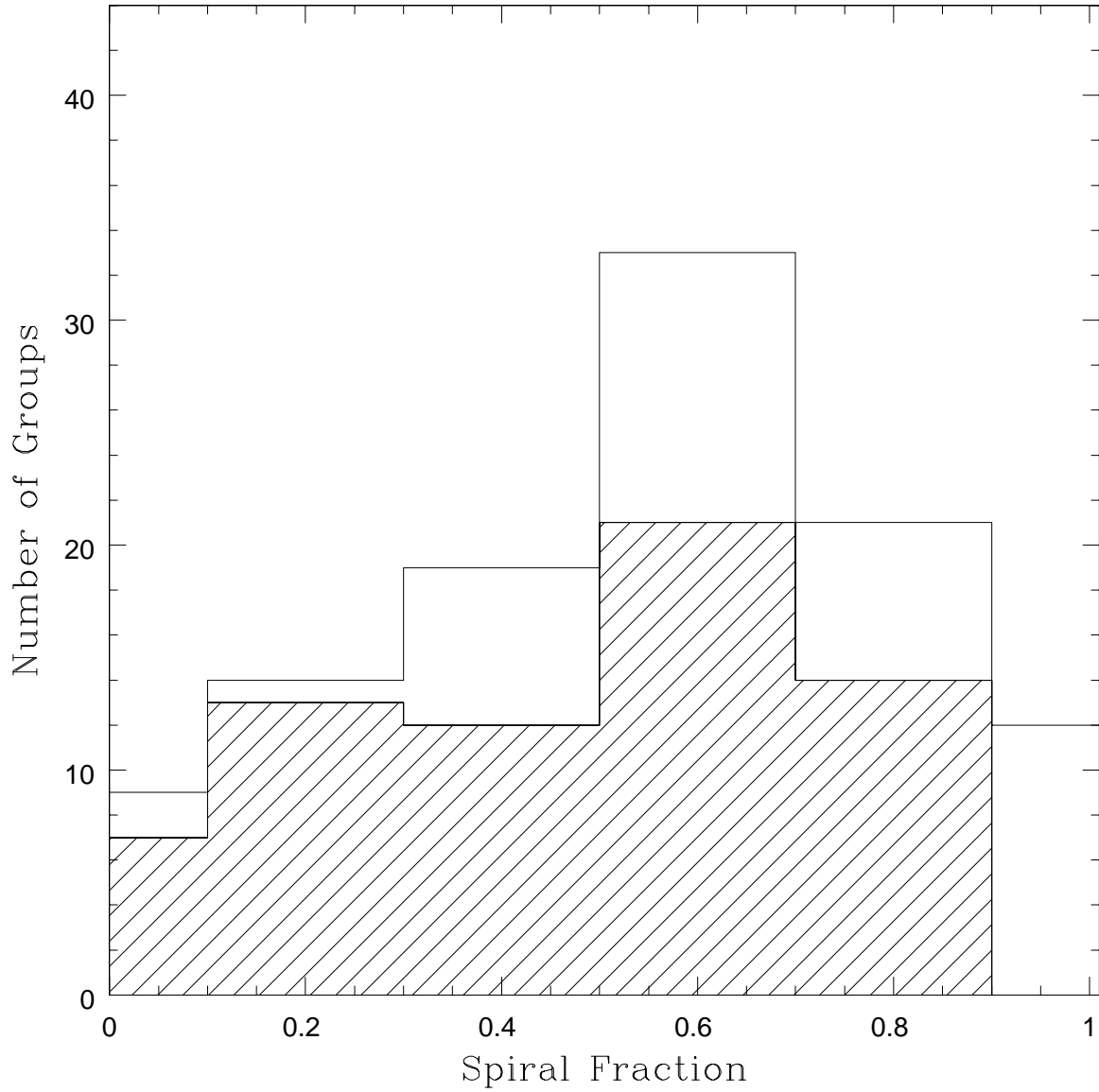


Fig. 12.— Histogram of spiral fraction for the entire group sample (open) and for the X-ray detected groups (filled). The 6 marginally detected groups are included in the X-ray detected group histogram. Note that no spiral-only group is detected in our survey.

Table 1. Group Sample

Group	RA (J2000)	Dec (J2000)	N_{gal}	z	σ km/s	f_{spiral}	ref	Catalog Name ¹
NGC 7805	00 02 28.0	+31 28 42.1	3	0.0164	71	0.66	1	G1/GH176/N173
NGC 43	00 13 05.8	+30 58 40.8	3	0.0160	63	0.33	1	G1/N1
HCG 2	00 31 30.0	+08 25 52.5	3	0.0144	55	1.00	2,3	H2
HCG 4	00 34 16.0	-21 26 48.0	5	0.0245	775	0.66	4,5	H4
HCG 3	00 34 27.5	-07 35 34.2	3	0.0255	251	0.33	2,3	H3
IC 1559	00 36 38.3	+23 58 30.2	3	0.0158	470	0.33	6	GH5
NGC 315	00 57 48.9	+30 21 08.8	4	0.0164	122	0.25	1	G14/GH8/N6
NGC 326	00 58 22.3	+26 52 03.7	9	0.0477	674	0.00	5,7	-
NGC 383	01 07 25.0	+32 24 45.2	40	0.0173	567	0.50	8,6	G18/GH9
NGC 491	01 20 42.3	-34 01 17.3	6	0.0126	86	1.00	9	MDL58
NGC 507	01 23 40.0	+33 15 20.0	21	0.0170	179	0.82	10	G26
NGC 524	01 24 47.8	+09 32 19.0	8	0.0083	205	0.50	1	G23/GH13/N11
NGC 533	01 25 31.4	+01 45 32.8	36	0.0181	464	0.39	9	GH14
HCG 10	01 26 07.4	+34 41 27.4	4	0.0161	209	0.75	2,3	G26/H10
HCG 12	01 27 33.2	-04 40 40.3	5	0.0485	240	0.20	2,3	H12
NGC 584	01 33 21.5	-07 01 16.5	4	0.0066	107	0.63	10	G27/HG45
NGC 664	01 44 02.7	+04 19 02	6	0.0180	130	1.00	9	-
NGC 720	01 53 00.5	-13 44 18.4	4	0.0059	161	0.75	10	G38
NGC 741	01 56 21.0	+05 37 44.2	41	0.0185	432	0.44	9	N20
HCG 15	02 07 37.6	+02 10 40.8	6	0.0228	427	0.50	2,3	H15
HCG 16	02 09 27.1	-10 07 37.2	9	0.0131	85	0.86	8,4,5	G49/H16
UGC 1651	02 09 38.2	+35 47 49.8	3	0.0363	111	0.00	5	-
HCG 18	02 39 06.8	+18 22 59.1	3	0.0137	31	1.00	5	H18
NGC 1044	02 41 06.3	+08 44 18.2	13	0.0205	325	0.66	5	-
IC 1860	02 49 33.4	-31 11 27.1	28	0.0231	452	0.32	5	MDL67
HCG 22	03 03 31.3	-15 40 32.5	8	0.0090	183	0.75	4,5,8	G81/H22
IC 1880	03 06 28.4	-09 43 42.5	7	0.0338	208	0.50	5	-
HCG 23	03 07 06.5	-09 35 07.7	14	0.0152	339	0.40	8,4,5	H23
HCG 26	03 21 54.2	-13 38 45.1	7	0.0316	200	0.57	2,3	H26
NGC 1332	03 26 17.1	-21 20 05.1	6	0.0052	347	0.50	5	G97/HG32
UGC 2755	03 29 24.0	+39 47 35.2	5	0.0230	406	0.66	5	-
NGC 1399	03 38 29.3	-35 27 02.3	55	0.0036	312	0.55	11	G96/HG17/MDL52

Table 1—Continued

Group	RA (J2000)	Dec (J2000)	N_{gal}	z	σ km/s	f_{spiral}	ref	Catalog Name ¹
NGC 1407	03 40 16.4	-18 35 41.7	8	0.0057	145	0.25	10	G100/HG32
NGC 1587	04 30 40.6	+00 40 00.6	4	0.0122	106	0.50	1	G117/N33
HCG 31	05 01 40.3	-01 15 24.3	11	0.0131	141	1.00	8,2,3	G123/H31
HCG 33	05 10 47.9	+18 02 04.7	4	0.0260	155	0.25	2,3	H33
NGC 1961	05 43 51.8	+69 18 09.4	4	0.0139	139	1.00	10	G132
NGC 2300	07 32 14.2	+85 42 33.7	13	0.0069	228	0.66	5,8	G145/HG92
NGC 2484	07 58 28.2	+37 47 12.9	2	0.0415	-	0.00	5	-
NGC 2563	08 20 35.7	+21 04 03.9	44	0.0159	419	0.72	12	G158
HCG 35	08 45 19.0	+44 30 54.7	6	0.0542	316	0.20	2,3	H35
NGC 2769	09 10 22.8	+50 23 45.3	3	0.0166	125	1.00	1	G168/N35
HCG 37	09 13 47.3	+30 00 37.1	5	0.0223	398	0.40	2,3	GH42/H37
NGC 2805	09 23 12.8	+63 47 09.0	4	0.0055	69	0.50	1	G186/GH46/N36
HCG 38	09 27 38.9	+12 16 50.9	3	0.0292	13	1.00	2,3	H38
HCG 40	09 38 54.5	-04 51 05.1	7	0.0221	280	0.50	4,5	H40
HCG 42	10 00 14.3	-19 38 13.3	35	0.0128	266	0.57	12	G186/HG37/H42
HCG 44	10 18 00.5	+21 48 44.1	4	0.0046	135	0.50	2,3	G194/H44/N43
MKW 2	10 30 10.4	-03 09 55.0	33	0.0365	603	0.20	5	-
HCG 48	10 37 50.0	-27 07 17.5	3	0.0094	302	0.33	2,3	G210/H48
CGCG154-041	10 43 18.7	+31 31 07.0	4	0.0350	312	-	5	-
NGC 3396	10 50 41.1	+33 13 17.3	6	0.0053	73	1.00	10	G218/GH67/HG65/N 55
NGC 3557	11 09 57.4	-37 32 17.1	22	0.0095	282	0.63	5,12	G229
NGC 3607	11 16 54.1	+18 03 18.9	7	0.0037	92	0.86	1	N66
HCG 50	11 17 06.1	+54 55 06.7	5	0.1391	468	0.00	2,3	H50
NGC 3647	11 21 45.8	+02 51 40.0	6	0.0495	383	0.00	5	-
NGC 3665	11 24 43.5	+38 45 43.4	4	0.0069	29	0.25	1	G236/GH79/N68
HCG 57	11 37 52.9	+21 58 17.8	7	0.0304	269	0.43	2,3	H57
HCG 58	11 42 10.8	+10 18 24.0	5	0.0206	215	0.60	1	H58/N82
NGC 3923	11 51 01.6	-28 48 19.9	5	0.0046	98	0.40	10	G255
NGC 4065	12 04 09.1	+20 17 06.0	7	0.0232	482	0.43	1	N91
NGC 4073	12 04 27.4	+01 53 42.4	19	0.0201	698	0.22	5	-
NGC 4104	12 06 45.4	+28 10 11.9	8	0.0286	423	0.14	5	-
NGC 4125	12 08 06.6	+65 10 28.9	3	0.0050	58	0.66	10	G274/GH94

Table 1—Continued

Group	RA (J2000)	Dec (J2000)	N_{gal}	z	σ km/s	f_{spiral}	ref	Catalog Name ¹
NGC 4168	12 13 38.9	+13 01 19.3	4	0.0077	152	0.50	1	N98
NGC 4261	12 19 23.5	+05 49 36.4	8	0.0068	108	0.50	10	G278/GH106/HG41/N99
SHK 202	12 19 44.2	+28 26 35.2	5	0.0267	600	0.00	5	-
NGC 4278	12 20 06.8	+29 16 50.7	17	0.0032	191	0.71	10	G279/GH94/HG60/N100
NGC 4357	12 20 51.1	+49 18 21.7	3	0.0142	273	0.66	6	GH103
NGC 4325	12 23 06.6	+10 37 13.2	26	0.0254	328	0.66	12	-
NGC 4291	12 24 41.2	+75 19 56.4	11	0.0068	132	0.73	10	G284/GH107/HG88
NGC 4615	12 41 16.0	+26 13 33.1	3	0.0158	47	0.33	1	N108
NGC 4636	12 42 49.8	+02 41 14.3	12	0.0044	463	0.83	1	N104
HCG 62	12 53 06.1	-09 12 16.3	63	0.0145	390	0.47	12	H62
NGC 5044	13 15 26.1	-16 23 01.7	9	0.0082	119	0.56	10	G338
NGC 5101	13 18 57.0	-26 53 39.5	10	0.0062	144	0.80	10	G341/HG31
NGC 5129	13 24 10.0	+13 58 42.3	38	0.0233	304	0.65	12	GH117/N117
NGC 5171	13 29 24.3	+11 44 11.9	15	0.0232	477	0.00	5	-
NGC 5218	13 32 42.3	+62 34 41.5	3	0.0103	132	0.66	10	G354/GH122/N120
IC 4296	13 36 41.5	-34 00 32.4	29	0.0125	228	0.69	13	-
HCG 67	13 49 12.3	-07 12 34.3	14	0.0248	351	0.50	4,5	H67
NGC 5322	13 49 14.7	+60 11 27.4	8	0.0065	196	0.37	1	G360/N123
HCG 68	13 53 27.1	+40 16 55.9	5	0.0080	155	0.20	2,3	G363/H68/N124
NGC 5374	13 58 00.1	+06 15 25.0	3	0.0143	9	0.33	1	G368/GH127/N129
NGC 5775	14 53 24.9	+03 29 47.5	5	0.0051	88	0.80	1	G387/GH148/N143
NGC 5846	15 06 29.4	+01 36 12.3	20	0.0063	368	0.73	9	G393/GH150/HG50/N146
NGC 5866	15 16 23.7	+56 25 01.9	4	0.0022	74	0.75	1	G396/GH152/HG78/N147
NGC 5929	15 26 18.1	+41 05 34.2	3	0.0086	66	1.00	1	G399/GH153/N150
NGC 5970	15 36 16.2	+12 02 07.7	3	0.0064	81	1.00	1	G401/GH157/N154
NGC 6052	15 59 31.1	+20 32 33.0	11	0.0154	183	0.82	10	G403/GH161/N158
NGC 6109	16 17 26.9	+34 55 23.5	53	0.0312	563	0.53	15	-
NGC 6251	16 32 32.3	+82 32 15.0	2	0.0221	-	0.00	5	-
HCG 84	16 44 08.1	+77 50 09.3	5	0.0556	204	0.20	2,3	H84
ARP 330	16 49 11.8	+53 25 12.0	8	0.0298	369	0.20	5	-
NGC 6269	16 57 54.4	+27 52 17.8	46	0.0353	586	0.35	8,5	-
NGC 6329	17 14 14.4	+43 41 01.2	13	0.0274	419	0.83	5	-

Table 1—Continued

Group	RA (J2000)	Dec (J2000)	N_{gal}	z	σ km/s	f_{spiral}	ref	Catalog Name ¹
NGC 6338	17 15 22.9	+57 24 38.1	11	0.0284	538	0.38	5	-
HCG 90	22 01 59.5	-31 57 50.4	16	0.0085	193	0.75	9	H90/G450/MDL59
UGC 12064	22 31 21.3	+39 21 21.7	9	0.0166	399	0.75	5	-
HCG 92	22 35 59.0	+33 57 11.9	4	0.0215	389	0.75	2,3	G459/H92
NGC 7358	22 46 44.2	-65 04 10.5	3	0.0098	113	0.00	11	G462/MDL5
IC 1459	22 57 10.4	-36 27 37.4	5	0.0057	80	0.80	10	G466/HG15
NGC 7448	23 01 04.9	+15 52 07.9	6	0.0068	116	0.33	1	G469/N160
HCG 93	23 15 24.2	+18 58 59.2	4	0.0168	209	0.50	2,3	H93
NGC 7582	23 18 15.3	-42 31 08.2	8	0.0054	38	1.00	9	G472/HG12
NGC 7619	23 20 14.8	+08 12 27.7	7	0.0116	253	0.14	1	G473/GH166/N164
HCG 96	23 27 58.3	+08 46 26.6	4	0.0292	132	0.75	2,3	H96
HCG 97	23 47 23.2	-02 18 07.4	14	0.0221	425	0.50	4,5	H97
NGC 7777	23 53 09.1	+28 15 44.3	4	0.0229	116	0.25	1	N170

Note. — ¹ G=Garcia (1993), GH=Geller & Huchra (1983), H=Hickson (1982), HG=Huchra & Geller (1982), MDL=Maia, Da Costa & Latham (1989), N=Nolthenius (1993)

Note. — references: 1) Nolthenius 1993, 2) Hickson et al. 1992, 3) Hickson, Kindl and Auman 1989, 4) Ribeiro et al. 1998 5) NASA Extragalactic Database (NED), 6) Geller and Huchra 1983, 7) Werner et al. 1999, 8) Zimer, Zabludoff and Mulchaey (2002), 9) Zabludoff and Mulchaey (1998), 10) Garcia 1993, 11) Maia, Da Costa and Latham 1989, 12) Zabludoff and Mulchaey (2000), 13) Willmer et al. 1999, 14) Willmer et al. 1991, 15) Mahdavi et al. 1999.

Table 2. X-ray Properties

Group	Exposure (sec)	Detection	N_{H} (cm^{-2})	R_{X} (arcmin/kpc)	T (keV)	Abundance (solar)	D (Mpc)	Log L_{x} (erg/s)
NGC 7805	13,995	UL	5.6	-	-	-	46.4	<40.31
NGC 43	7,822	UL	5.5	-	-	-	45.2	<40.85
HCG 2	18,633	UL	4.3	-	-	-	40.0	<40.85
HCG 4	8,852	UL	1.6	-	-	-	71.7	<41.11
HCG 3	7,156	UL	3.6	-	-	-	78.6	<41.54
IC 1559	6,841	UL	3.4	-	-	-	44.5	<40.90
NGC 315	25,939	DE/AGN	5.9	5/66	$0.80^{+0.18}_{-0.14}$ $0.81^{+0.19}_{-0.12}$	$0.06^{+0.09}_{-0.04}$ (0.3)	46.6	$41.57^{+0.10}_{-0.08}$
NGC 326	19,680	DE	5.8	19/734	$1.41^{+0.72}_{-0.37}$ $1.41^{+0.47}_{-0.24}$	$0.32^{+0.55}_{-0.23}$ (0.3)	144.8	$42.97^{+0.12}_{-0.12}$
NGC 383	28,220	DE	5.4	30/442	$1.51^{+0.21}_{-0.11}$ $3.37^{+0.59}_{-0.55}$	$0.12^{+0.10}_{-0.07}$ (0.3)	49.5	$42.72^{+0.05}_{-0.04}$
NGC 491	10,450	UL	2.3	-	-	-	35.7	<40.70
NGC 507	17,878	DE	5.2	33/455	$1.25^{+0.08}_{-0.07}$ $1.30^{+0.05}_{-0.05}$	$0.22^{+0.06}_{-0.05}$ (0.3)	48.7	$42.95^{+0.03}_{-0.03}$
NGC 524	10,560	DE	4.5	9/57	$0.47^{+0.24}_{-0.19}$	(0.3)	21.9	$40.53^{+0.37}_{-0.47}$
NGC 533	11,779	DE	3.1	18/263	$1.03^{+0.06}_{-0.08}$ $1.00^{+0.07}_{-0.09}$	$0.59^{+0.86}_{-0.26}$ (0.3)	51.8	$42.37^{+0.24}_{-0.13}$
HCG 10	14,131	UL	4.9	-	-	-	46.0	<40.67
HCG 12	8,923	DE	3.6	5/197	$0.67^{+0.61}_{-0.31}$	(0.3)	147.5	$41.88^{+0.20}_{-0.45}$
NGC 584	3,706	UL	3.8	-	-	-	16.9	<40.51
NGC 664	7,531	UL	3.4	-	-	-	52.3	<40.98
NGC 720	22,487	DE	1.5	9/39	$0.51^{+0.07}_{-0.05}$ $0.53^{+0.06}_{-0.05}$	$0.09^{+0.06}_{-0.04}$ (0.3)	15.1	$40.86^{+0.09}_{-0.07}$
NGC 741	12,865	DE	4.5	16/240	$1.06^{+0.13}_{-0.12}$ $1.08^{+0.13}_{-0.09}$	$0.22^{+0.22}_{-0.11}$ (0.3)	53.4	$42.14^{+0.11}_{-0.09}$
HCG 15	13,228	DE?	3.2	9/168	$1.26^{+0.53}_{-0.33}$	(0.3)	66.8	$41.72^{+0.18}_{-0.22}$
HCG 16	14,000	DE	2.2	11/118	$0.37^{+0.40}_{-0.14}$	(0.3)	37.1	$40.74^{+0.38}_{-0.49}$
UGC 1651	13,424	DE	6.1	11/328	1.43*	(0.3)	109.3	$42.15^{+0.16}_{-0.22}$
HCG 18	2,942	UL	8.6	-	-	-	39.1	<41.04
NGC 1044	16,184	DE	8.8	8/141	$0.87^{+0.61}_{-0.29}$	$0.06^{+0.62}_{-0.06}$	62.8	$41.69^{+0.42}_{-0.13}$

Table 2—Continued

Group	Exposure (sec)	Detection	N_{H} (cm^{-2})	R_{X} (arcmin/kpc)	T (keV)	Abundance (solar)	D (Mpc)	Log L_{x} (erg/s)
IC 1860	9,180	DE	2.1	18/345	$0.99^{+0.74}_{-0.33}$ $1.14^{+0.20}_{-0.11}$ $1.26^{+0.14}_{-0.17}$	(0.3) $0.17^{+0.14}_{-0.07}$ (0.3)	68.8	$42.75^{+0.06}_{-0.06}$
HCG 22	12,298	DE?	4.2	-	-	-	25.4	<40.37
IC 1880	4,122	DE	6.5	7/196	$1.13^{+0.20}_{-0.16}$	(0.3)	102.0	$42.34^{+0.22}_{-0.24}$
HCG 23	4,122	UL	6.5	-	-	-	44.3	<40.96
HCG 26	5,011	UL	5.4	-	-	-	95.4	<41.26
NGC 1332	25,051	UL	2.2	-	-	-	14.2	<40.04
UGC 2755	16,826	DE	14.3	7/134	$0.66^{+0.22}_{-0.21}$	(0.3)	68.6	$41.60^{+0.33}_{-0.41}$
NGC 1399	26,954	DE	1.3	40/115	$1.38^{+0.03}_{-0.03}$ $1.39^{+0.02}_{-0.02}$	$0.28^{+0.04}_{-0.04}$ (0.3)	9.9	$41.94^{+0.04}_{-0.03}$
NGC 1407	18,222	DE	5.4	15/69	$0.95^{+0.09}_{-0.07}$ $1.02^{+0.06}_{-0.07}$	$0.14^{+0.10}_{-0.05}$ (0.3)	15.9	$41.23^{+0.07}_{-0.05}$
NGC 1587	8,080	DE	6.5	6/62	$0.90^{+0.81}_{-0.46}$	(0.3)	36.2	$40.92^{+0.13}_{-0.41}$
HCG 31	1,584	UL	6.0	-	-	-	39.5	<40.97
HCG 33	4,081	DE?	22.0	-	-	-	79.3	<41.45
NGC 1961	10,703	UL	8.3	-	-	-	41.8	<40.84
NGC 2300	17,232	DE	5.1	25/135	$0.87^{+0.12}_{-0.09}$ $1.05^{+0.06}_{-0.07}$	$0.04^{+0.03}_{-0.02}$ (0.3)	20.5	$41.62^{+0.04}_{-0.04}$
NGC 2484	15,504	DE/AGN	5.1	7/249	$0.86^{+0.63}_{-0.38}$ $1.04^{+0.92}_{-0.34}$	$0.04^{+0.31}_{-0.04}$ (0.3)	130.1	$42.41^{+0.21}_{-0.15}$
NGC 2563	21,155	DE	4.3	18/258	$1.09^{+0.10}_{-0.10}$ $1.11^{+0.15}_{-0.07}$	$0.18^{+0.13}_{-0.07}$ (0.3)	50.6	$42.16^{+0.07}_{-0.06}$
HCG 35	15,262	DE?	2.8	-	-	-	171.1	<41.84
NGC 2769	8,773	UL	1.6	-	-	-	52.1	<40.82
HCG 37	4,884	DE	1.6	8/157	$0.65^{+0.29}_{-0.32}$	(0.3)	70.6	$41.63^{+0.31}_{-0.46}$
NGC 2805	5,931	UL	3.9	-	-	-	17.6	<40.46
HCG 38	7,692	UL	3.5	-	-	-	92.8	<41.40
HCG 40	9,459	UL	3.5	-	-	-	70.9	<41.05
HCG 42	11,799	DE	4.8	9/108	$0.73^{+0.08}_{-0.06}$	(0.3)	42.3	$41.59^{+0.32}_{-0.34}$
HCG 44	4,543	UL	2.1	-	-	-	17.0	<40.70

Table 2—Continued

Group	Exposure (sec)	Detection	N_{H} (cm^{-2})	R_{X} (arcmin/kpc)	T (keV)	Abundance (solar)	D (Mpc)	Log L_{x} (erg/s)
MKW 2	9,017	DE	4.4	9/286	$1.31^{+0.89}_{-0.28}$	(0.3)	116.3	$42.32^{+0.13}_{-0.21}$
HCG 48	17,972	DE?	5.1	6/54	$2.56^{+2.4}_{-0.75}$	(0.3)	31.9	$41.39^{+0.19}_{-0.13}$
CGCG154-041	20,581	DE	1.9	8/242	$1.05^{+0.32}_{-0.22}$	(0.3)	110.7	$41.99^{+0.20}_{-0.28}$
NGC 3396	15,493	UL	2.0	-	-	-	18.8	$<40.49^1$
NGC 3557	19,219	DE	7.4	8/73	$0.25^{+0.08}_{-0.04}$	(0.3)	31.9	$41.12^{+0.32}_{-0.58}$
NGC 3607	23,143	DE	1.6	10/42	$0.40^{+0.06}_{-0.05}$	(0.3)	14.5	$40.53^{+0.38}_{-0.42}$
HCG 50	1,175	UL	0.8	-	-	-	461.9	<42.55
NGC 3647	13,691	DE	4.3	18/759	$1.46^{+0.62}_{-0.33}$	$0.02^{+0.09}_{-0.02}$	157.9	$43.37^{+0.24}_{-0.11}$
					$2.21^{+0.98}_{-0.49}$	(0.3)		
NGC 3665	6,613	DE	2.1	6/40	$0.33^{+0.14}_{-0.07}$	(0.3)	23.4	$40.63^{+0.37}_{-0.47}$
HCG 57	10,640	DE?	2.0	8/203	$1.14^{+1.93}_{-0.31}$	(0.3)	96.6	$41.92^{+0.14}_{-0.27}$
HCG 58	11,321	UL	3.2	-	-	-	66.4	$<40.88^1$
NGC 3923	36,697	DE	6.2	8/40	$0.52^{+0.12}_{-0.13}$	(0.3)	17.3	$40.29^{+0.37}_{-0.42}$
NGC 4065	15,422	DE	2.4	17/351	$1.20^{+0.19}_{-0.13}$	(0.3)	74.1	$42.40^{+0.21}_{-0.22}$
NGC 4073	9,697	DE	1.9	22/404	$1.75^{+0.24}_{-0.15}$	$1.14^{+0.72}_{-0.43}$	64.9	$43.04^{+0.09}_{-0.08}$
					$1.44^{+0.12}_{-0.06}$	(0.3)		
NGC 4104	13,891	DE	1.7	17/427	$1.46^{+0.31}_{-0.16}$	$0.29^{+0.29}_{-0.14}$	90.7	$42.77^{+0.08}_{-0.06}$
					$1.48^{+0.24}_{-0.14}$	(0.3)		
NGC 4125	3,900	DE	1.9	6/28	$0.44^{+0.18}_{-0.11}$	(0.3)	16.1	$40.54^{+0.38}_{-0.43}$
NGC 4168	13,824	UL	2.6	-	-	-	26.6	<40.56
NGC 4261	19,163	DE	1.5	27/187	$0.91^{+0.17}_{-0.11}$	$0.03^{+0.04}_{-0.03}$	24.0	$41.89^{+0.07}_{-0.05}$
					$1.29^{+0.11}_{-0.11}$	(0.3)		
SHK 202	11,563	DE	1.9	15/340	$0.77^{+0.29}_{-0.20}$	(0.3)	81.6	$42.01^{+0.27}_{-0.37}$
NGC 4278	3,228	UL	1.8	-	-	-	12.5	$<40.83^1$
NGC 4357	3,139	UL	1.3	-	-	-	45.0	<41.37
NGC 4325	4,984	DE	2.2	9/203	$0.81^{+0.04}_{-0.04}$	$0.45^{+0.44}_{-0.17}$	81.1	$42.80^{+0.19}_{-0.11}$
					$0.81^{+0.04}_{-0.05}$	(0.3)		
NGC 4291	11,502	DE	2.8	14/84	$0.49^{+0.25}_{-0.20}$	(0.3)	20.9	$40.74^{+0.37}_{-0.46}$
NGC 4615	4,845	UL	1.2	-	-	-	50.9	<41.00
NGC 4636	11,737	DE	1.8	22/105	$0.74^{+0.04}_{-0.03}$	$0.41^{+0.40}_{-0.12}$	16.6	$41.88^{+0.20}_{-0.08}$
					$0.73^{+0.03}_{-0.03}$	(0.3)		

Table 2—Continued

Group	Exposure (sec)	Detection	N_{H} (cm^{-2})	R_{X} (arcmin/kpc)	T (keV)	Abundance (solar)	D (Mpc)	Log L_{x} (erg/s)
HCG 62	17,711	DE	3.0	29/389	$0.96^{+0.08}_{-0.08}$ $1.08^{+0.05}_{-0.05}$	$0.09^{+0.06}_{-0.04}$ (0.3)	47.4	$42.69^{+0.05}_{-0.05}$
NGC 5044	26,097	DE	5.0	36/287	$1.02^{+0.02}_{-0.02}$ $1.05^{+0.01}_{-0.02}$	$0.20^{+0.03}_{-0.03}$ (0.3)	27.9	$42.81^{+0.02}_{-0.02}$
NGC 5101	5,278	UL	5.7	-	-	-	21.7	<40.77
NGC 5129	5,568	DE	1.8	9/187	$0.81^{+0.12}_{-0.10}$	(0.3)	74.1	$42.16^{+0.31}_{-0.33}$
NGC 5171	4,616	DE	1.9	14/288	$1.25^{+0.40}_{-0.25}$	(0.3)	73.8	$42.35^{+0.17}_{-0.23}$
NGC 5218	5,653	UL	2.0	-	-	-	32.1	<40.93
IC 4296	3,774	DE	4.1	15/173	$0.85^{+0.33}_{-0.24}$	(0.3)	40.6	$41.85^{+0.24}_{-0.35}$
HCG 67	15,093	DE	2.5	10/219	$0.78^{+0.32}_{-0.22}$	(0.3)	78.8	$41.65^{+0.26}_{-0.37}$
NGC 5322	26,585	DE	1.8	5/29	$0.33^{+0.19}_{-0.07}$	(0.3)	20.6	$40.10^{+0.38}_{-0.47}$
HCG 68	11,780	DE	1.0	10/75	$0.59^{+0.10}_{-0.11}$	(0.3)	26.0	$40.99^{+0.36}_{-0.39}$
NGC 5374	5,556	UL	2.1	-	-	-	46.1	<41.05
NGC 5775	5,913	UL	3.5	-	-	-	17.4	<40.62
NGC 5846	6,979	DE	4.2	15/90	$0.70^{+0.05}_{-0.04}$ $0.70^{+0.04}_{-0.04}$	$0.31^{+0.28}_{-0.12}$ (0.3)	20.9	$41.71^{+0.17}_{-0.11}$
NGC 5866	16,332	UL	1.5	-	-	-	7.2	<39.48 ¹
NGC 5929	10,347	UL	2.0	-	-	-	26.9	<40.50
NGC 5970	6,866	UL	3.5	-	-	-	20.6	<41.37
NGC 6052	4,728	UL	4.0	-	-	-	47.6	<41.13
NGC 6109	6,020	DE	1.4	25/662	$2.22^{+1.20}_{-0.58}$ $2.43^{+1.28}_{-0.53}$	$0.13^{+0.43}_{-0.13}$ (0.3)	96.2	$43.21^{+0.14}_{-0.10}$
NGC 6251	13,699	DE/AGN	5.5	10/187	$0.87^{+0.25}_{-0.17}$	(0.3)	67.0	$41.82^{+0.26}_{-0.33}$
HCG 84	35,363	UL	4.0	-	-	-	173.3	<41.93
ARP 330	6,794	DE	2.7	10/252	$1.29^{+0.14}_{-0.20}$	(0.3)	91.2	$42.57^{+0.20}_{-0.21}$
NGC 6269	10,345	DE	4.7	23/703	$1.83^{+0.62}_{-0.27}$ $1.92^{+0.44}_{-0.26}$	$0.27^{+0.33}_{-0.16}$ (0.3)	108.7	$43.20^{+0.09}_{-0.07}$
NGC 6329	17,995	DE	2.1	16/370	$0.99^{+0.10}_{-0.12}$ $1.03^{+0.09}_{-0.10}$	$0.16^{+0.15}_{-0.08}$ (0.3)	83.5	$42.45^{+0.09}_{-0.08}$
NGC 6338	4,006	DE	2.6	15/359	$1.82^{+0.90}_{-0.40}$ $2.02^{+0.83}_{-0.37}$	$0.19^{+0.32}_{-0.15}$ (0.3)	86.6	$43.25^{+0.11}_{-0.09}$

Table 2—Continued

Group	Exposure (sec)	Detection	N_{H} (cm^{-2})	R_{X} (arcmin/kpc)	T (keV)	Abundance (solar)	D (Mpc)	Log L_{x} (erg/s)
HCG 90	17,146	DE	1.6	10/66	$0.51^{+0.15}_{-0.14}$	(0.3)	22.9	$40.60^{+0.37}_{-0.42}$
UGC 12064	9,068	DE	11.8	15/200	$1.03^{+0.14}_{-0.14}$	(0.3)	47.2	$42.17^{+0.26}_{-0.27}$
HCG 92	18,695	DE	8.3	5/92	$1.05^{+0.89}_{-0.30}$	(0.3)	65.2	$41.31^{+0.12}_{-0.30}$
NGC 7358	11,064	UL	2.5	-	-	-	28.4	<40.59
IC 1459	31,139	DE	1.2	12/50	$0.63^{+0.06}_{-0.06}$	(0.3)	14.4	$40.52^{+0.36}_{-0.36}$
NGC 7448	6,762	UL	6.1	-	-	-	17.8	<40.40
HCG 93	15,022	UL	4.7	-	-	-	47.3	<40.65
NGC 7582	7,028	UL	1.9	-	-	-	13.7	<40.74 ¹
NGC 7619	17,943	DE	5.0	23/96	$0.98^{+0.07}_{-0.07}$ $1.05^{+0.05}_{-0.05}$	$0.12^{+0.06}_{-0.04}$ (0.3)	31.3	$42.05^{+0.05}_{-0.04}$
HCG 96	2,480	UL	5.2	-	-	-	85.6	<41.64
HCG 97	12,092	DE	3.7	11/196	$0.97^{+0.14}_{-0.12}$ $1.02^{+0.11}_{-0.12}$	$0.16^{+0.10}_{-0.09}$ (0.3)	63.6	$42.06^{+0.07}_{-0.10}$
NGC 7777	16,924	DE	5.0	7/130	$0.63^{+0.52}_{-0.20}$	(0.3)	66.3	$41.28^{+0.25}_{-0.42}$

Note. — ¹ Extraction radius for the X-ray luminosity is less than 200 kpc: NGC 3396 (194 kpc), HCG 58 (83 kpc), NGC 4278 (148 kpc), NGC 5866 (76 kpc), NGC 7582 (120 kpc).

Table 3. Spatial Fits

Group	Extended Component			Central Component	
	R_{core} (arcminute)	β	ellipticity	R_{core} (arcminute)	β
NGC 315	0.23 ± 0.02	0.77 ± 0.02	$0.00^{+0.05}_{-0.00}$	-	-
NGC 326	2.00 ± 0.15	0.36 ± 0.01	$0.05^{+0.11}_{-0.05}$	-	-
	2.22 ± 0.19	0.35 ± 0.01	$0.09^{+0.11}_{-0.09}$	0.11 ± 0.02	0.50 ± 0.04
NGC383	<0.1	0.32 ± 0.01	0.13 ± 0.04	-	-
	<0.1	0.42 ± 0.01	0.12 ± 0.05	0.22 ± 0.01	(1.0)
NGC 507	1.28 ± 0.03	0.46 ± 0.01	0.09 ± 0.03	-	-
	1.27 ± 0.03	0.42 ± 0.01	0.09 ± 0.03	<0.1	(1.0)
NGC 524	<0.1	0.41 ± 0.02	$0.15^{+0.18}_{-0.15}$	-	-
NGC 533	<0.1	0.46 ± 0.01	0.10 ± 0.05	-	-
	0.42 ± 0.02	0.95 ± 0.04	0.21 ± 0.05	<0.1	0.36 ± 0.01
HCG 12	<0.1	0.34 ± 0.02	$0.53^{+0.25}_{-0.34}$	-	-
NGC 720	<0.1	0.41 ± 0.01	0.15 ± 0.05	-	-
	0.44 ± 0.02	0.65 ± 0.01	0.14 ± 0.05	<0.1	0.31 ± 0.01
NGC 741	<0.1	0.43 ± 0.01	$0.00^{+0.08}_{-0.00}$	-	-
	<0.1	0.43 ± 0.01	$0.00^{+0.08}_{-0.00}$	<0.1	(1.0)
HCG 15	<0.1	0.34 ± 0.01	$0.18^{+0.25}_{-0.18}$	-	-
HCG 16	<0.1	0.35 ± 0.03	(0.00)	-	-
UGC 1651	<0.1	0.33 ± 0.01	$0.21^{+0.16}_{-0.18}$	-	-
	<0.1	0.38 ± 0.01	0.19 ± 0.19	0.14 ± 0.02	$0.77^{+0.11}_{-0.07}$
NGC 1044	<0.1	0.38 ± 0.02	$0.26^{+0.22}_{-0.20}$	-	-
IC 1860	0.22 ± 0.01	0.46 ± 0.01	$0.00^{+0.04}_{-0.00}$	-	-
	0.32 ± 0.01	0.47 ± 0.02	$0.00^{+0.04}_{-0.00}$	0.30 ± 0.01	(1.0)
IC 1880	<0.1	(1.00)	(0.00)	-	-
UGC 2755	<0.1	0.36 ± 0.01	$0.11^{+0.13}_{-0.11}$	-	-
	<0.1	0.48 ± 0.02	$0.22^{+0.13}_{-0.13}$	<0.1	0.31 ± 0.01
NGC 1399	<0.1	0.39 ± 0.01	0.03 ± 0.01	-	-
	<0.1	0.38 ± 0.01	0.02 ± 0.01	0.32 ± 0.01	(1.0)
NGC 1407	0.20 ± 0.02	0.34 ± 0.01	0.23 ± 0.12	-	-
	0.60 ± 0.05	0.37 ± 0.01	0.22 ± 0.11	<0.1	(1.0)
NGC 1587	<0.1	0.42 ± 0.02	(0.00)	-	-

Table 3—Continued

Group	Extended Component			Central Component	
	R_{core} (arcminute)	β	ellipticity	R_{core} (arcminute)	β
NGC 2300	<0.1	(1.0)	$0.39^{+0.09}_{-0.06}$	-	-
NGC 2484	<0.1	0.53 ± 0.01	0.11 ± 0.09	-	-
NGC 2563	1.28 ± 0.11	0.33 ± 0.01	$0.15^{+0.11}_{-0.12}$	-	-
	1.29 ± 0.10	0.42 ± 0.01	0.14 ± 0.11	<0.1	(1.0)
HCG 37	<0.1	0.31 ± 0.03	(0.00)	-	-
HCG 42	0.13 ± 0.03	0.35 ± 0.01	(0.00)	-	-
	1.75 ± 0.70	0.41 ± 0.02	(0.00)	0.84 ± 0.45	(1.00)
MKW 2	<0.1	0.34 ± 0.02	$0.00^{+0.37}_{-0.00}$	-	-
	<0.1	0.33 ± 0.02	$0.17^{+0.36}_{-0.17}$	<0.1	(1.0)
HCG 48	0.85 ± 0.05	0.56 ± 0.01	$0.00^{+0.06}_{-0.00}$	-	-
CGCG154-041	<0.1	0.38 ± 0.01	0.14 ± 0.11	-	-
	<0.1	0.36 ± 0.01	0.15 ± 0.14	0.23 ± 0.05	(1.0)
NGC 3557	<0.1	0.44 ± 0.01	$0.00^{+0.13}_{-0.00}$	-	-
NGC 3607	<0.1	0.43 ± 0.01	0.20 ± 0.11	-	-
	<0.1	0.42 ± 0.01	(0.00)	<0.1	0.50 ± 0.02
NGC 3647	$2.51^{+0.24}_{-0.14}$	0.40 ± 0.01	$0.00^{+0.10}_{-0.00}$	-	-
	4.34 ± 0.35	0.46 ± 0.02	$0.10^{+0.10}_{-0.11}$	<0.1	(1.00)
NGC 3665	<0.1	0.42 ± 0.03	(0.00)	-	-
HCG 57	0.25 ± 0.10	0.34 ± 0.02	(0.00)	-	-
NGC 3923	<0.1	0.56 ± 0.01	$0.00^{+0.03}_{-0.00}$	-	-
	0.34 ± 0.01	0.89 ± 0.02	(0.00)	<0.1	0.35 ± 0.01
NGC 4065	$3.75^{+0.59}_{-0.16}$	0.42 ± 0.01	(0.00)	-	-
	$2.52^{+0.56}_{-0.46}$	0.46 ± 0.01	$0.45^{+0.15}_{-0.20}$	<0.1	0.31 ± 0.01
NGC 4073	<0.1	0.44 ± 0.01	0.15 ± 0.03	-	-
	<0.1	0.43 ± 0.01	0.19 ± 0.04	0.61 ± 0.04	(1.00)
NGC 4104	0.95 ± 0.07	0.38 ± 0.01	$0.00^{+0.09}_{-0.00}$	-	-
	0.95 ± 0.08	0.42 ± 0.01	$0.00^{+0.11}_{-0.00}$	<0.1	0.36 ± 0.01
NGC 4125	<0.1	0.47 ± 0.03	(0.00)	-	-
NGC 4261	<0.1	(1.00)	(0.00)	-	-
NGC 4325	0.40 ± 0.01	0.65 ± 0.01	$0.00^{+0.03}_{-0.00}$	-	-

Table 3—Continued

Group	Extended Component			Central Component	
	R_{core} (arcminute)	β	ellipticity	R_{core} (arcminute)	β
	0.90±0.03	1.13±0.06	(0.00)	<0.1	0.43±0.01
NGC 4636	0.16±0.01	0.43±0.01	0.00 ^{+0.01} _{-0.00}	-	-
	0.77±0.01	0.76±0.01	(0.00)	<0.1	0.33±0.01
HCG 62	<0.1	1.76 ^{+0.23} _{-0.17}	0.00 ^{+0.16} _{-0.00}	-	-
	<0.1	0.35±0.01	0.18±0.05	1.34±0.02	2.17 ^{+0.05} _{-0.08}
NGC 5044	1.28±0.01	0.52±0.01	0.00 ^{+0.03} _{-0.00}	-	-
	0.76±0.01	0.43±0.01	0.14±0.01	3.88±0.03	1.14±0.01
NGC 5129	<0.1	0.39±0.01	0.00 ^{+0.17} _{-0.00}	-	-
NGC 5171	0.28±0.11	0.32±0.02	0.29 ^{+0.32} _{-0.29}	-	-
IC 4296	3.47 ^{+1.65} _{-1.24}	0.35±0.03	(0.00)	-	-
HCG 67	<0.1	0.36±0.01	0.00 ^{+0.18} _{-0.00}	-	-
NGC 5322	<0.1	0.38±0.01	0.41±0.13	-	-
HCG 68	<0.1	0.43±0.01	0.32 ^{+0.28} _{-0.32}	-	-
NGC 5846	0.90±0.05	0.56±0.01	0.00 ^{+0.09} _{-0.00}	-	-
	<0.1	0.52±0.01	0.26 ^{+0.13} _{-0.12}	2.31±0.16	(1.0)
NGC 6109	2.48±0.41	0.43±0.02	0.00 ^{+0.16} _{-0.00}	-	-
	2.03±0.40	0.41±0.02	0.43 ^{+0.15} _{-0.18}	1.33±1.21	(1.00)
NGC 6251	<0.1	0.63±0.01	0.00 ^{+0.04} _{-0.00}	-	-
	<0.1	0.39±0.01	0.13 ^{+0.22} _{-0.13}	0.23±0.01	(1.0)
ARP 330	<0.1	0.35±0.01	0.00 ^{+0.20} _{-0.00}	-	-
NGC 6269	1.95±0.20	0.48±0.02	0.00 ^{+0.17} _{-0.00}	-	-
	2.03±0.21	0.47±0.02	0.03 ^{+0.15} _{-0.03}	<0.1	(1.0)
NGC 6329	1.02±0.13	0.45±0.01	0.00 ^{+0.15} _{-0.00}	-	-
	1.04±0.13	0.44±0.01	0.00 ^{+0.19} _{-0.00}	<0.1	(1.0)
NGC 6338	<0.1	0.44±0.01	0.07±0.07	-	-
	<0.1	0.50±0.01	0.00 ^{+0.11} _{-0.00}	0.38±0.04	(1.0)
HCG 90	0.84±0.24	0.95±0.07	0.22 ^{+0.27} _{-0.22}	-	-
UGC 12064	<0.1	0.38±0.03	0.04 ^{+0.15} _{-0.04}	-	-
	<0.1	0.43±0.01	0.00 ^{+0.16} _{-0.00}	<0.1	(1.0)
HCG 92	<0.1	0.43±0.03	0.35 ^{+0.18} _{-0.24}	-	-

Table 3—Continued

Group	Extended Component			Central Component	
	R_{core} (arcminute)	β	ellipticity	R_{core} (arcminute)	β
IC 1459	0.17 ± 0.01	0.66 ± 0.01	$0.00^{+0.04}_{-0.00}$	-	-
	0.15 ± 0.02	0.42 ± 0.01	$0.17^{+0.19}_{-0.17}$	0.32 ± 0.01	(1.0)
NGC 7619	0.51 ± 0.03	0.44 ± 0.01	$0.00^{+0.09}_{-0.00}$	-	-
	0.57 ± 0.03	0.54 ± 0.01	$0.19^{+0.07}_{-0.08}$	<0.1	(1.00)
HCG 97	<0.1	0.41 ± 0.01	$0.00^{+0.10}_{-0.00}$	-	-
	<0.1	0.48 ± 0.01	$0.48^{+0.16}_{-0.20}$	0.41 ± 0.04	0.77 ± 0.06
NGC 7777	<0.1	0.33 ± 0.03	(0.00)	-	-